



Description and osteohistology of two early immature enantiornithines (Aves: Ornithothoraces) from the Early Cretaceous Jehol Biota [☆]



Jingmai K. O'Connor^{a,b,*}, Jessie Atterholt^c, Alida M. Bailleul^b, Min Wang^b, Pei-Chen Kuo^a, Zhonghe Zhou^b

^a Negaunee Integrative Research Center, Field Museum of Natural History, Chicago, IL, 60605, USA

^b Key Laboratory of Vertebrate Evolution and Human Origins, Institute of Vertebrate Paleontology and Paleoanthropology, Chinese Academy of Sciences, Beijing, 10010, China

^c College of Osteopathic Medicine of the Pacific, Western University of Health Sciences, Pomona, CA, 91766, USA

ARTICLE INFO

Article history:

Received 9 November 2023

Revised 14 March 2024

Accepted 21 May 2024

Available online 6 August 2024

Keywords:

Enantiornithes

Stem-Aves

Bone microstructure

Osteohistology

Ontogeny

Mesozoic

ABSTRACT

The Enantiornithes is the dominant clade of Cretaceous land birds and the most diverse recognized clade of Mesozoic birds. More than half of this diversity is from the Lower Cretaceous Jehol deposits in north-eastern China, and numerous late immature and mature specimens have been sectioned for histological analysis. These specimens reveal thin cortices with low amounts of vascularization and variably-present growth lines. An inner circumferential layer is typically observed, but rarely a distinct outer circumferential layer. Here we describe the morphology and histology of two early immature enantiornithines and explore ontogenetic changes in skeletal morphology and bone formation. These specimens help to fill in a crucial ontogenetic gap between the previously sectioned embryonic specimen of *Gobipteryx* and purportedly mature or near mature specimens. In support of interpretations regarding the precocial onset of flight in Enantiornithes, the proportions of the forelimb cortical thicknesses relative to the hindlimb in IVPP V15575 is very similar to mature enantiornithines. Opposite neornithines, the bone tissue of the humerus is more mature than the tibia. Precocial development of the femur is considered plesiomorphic to Aves, thus the shift towards greater maturity in the forelimb relative to the hindlimb observed in IVPP V15575 probably reflects the apomorphic evolution of super-precocial flight in enantiornithines. Osteohistological traits in IVPP V15686 and V15575 resemble those of extant chicks on the more altricial end of the developmental mode spectrum, but individuals from later growth stages. Since ossification indicates these two specimens are very immature, this highlights the unique osteohistological development of enantiornithines. Differences between these two individuals are potentially indicative of inter-taxonomic variation in enantiornithine growth strategies. However, developmental plasticity in stem birds means that morphological and osteohistological maturity are decoupled and that ossification patterns can vary even within a taxon. As such, significantly more data are required to fully understand observed differences and extract patterns regarding variation in developmental strategy among enantiornithines.

© 2024 Elsevier Masson SAS. All rights are reserved, including those for text and data mining, AI training, and similar technologies.

1. Introduction

Histological research on stem-birds – non-neornithine avians, Aves *sensu* Sereno (2005) – began in the mid-1990's when Chinsamy et al. (1994) published femoral sections from two indeterminate enantiornithines and the basal ornithuromorph *Patagopteryx* (Chinsamy et al., 1994, 1995). This study revealed that these two Late Cretaceous, large-bodied enantiornithine taxa had protracted growth strategies, depositing avascular parallel fibered

bone tissue marked by lines of arrested growth (LAGs). In 1998 the first bird from the Jehol Biota was sampled – the femur of a specimen of the basal pygostylian *Confuciusornis* (Zhang et al., 1998). This taxon was soon restudied from numerous sections that sampled across the skeleton (de Ricqlès et al., 2003). Around the same time, histological studies were published on the tibia of a 'perinate' specimen of the Late Cretaceous enantiornithine *Gobipteryx* from Mongolia (Chinsamy and Elzanowski, 2001) and the tarsometatarsus of *Concornis*, an enantiornithine from the Early Cretaceous of Spain (Bailleul et al., 2011; Cambra-Moo et al., 2006). In 2009, Erickson and colleagues published a paper exploring the origin of avian growth rates, in which they sampled *Archaeopteryx*, *Jeholornis* (a long boney-tailed bird from the Jehol

[☆] Corresponding editor: Francisco J. Serrano.

* Corresponding author.

E-mail address: jingmai@fieldmuseum.org (J.K. O'Connor).

Biota), *Confuciusornis*, and *Sapeornis* (another basal pygostylian from the Jehol Biota; Erickson et al., 2009). *Sapeornis*, *Confuciusornis*, and *Jeholornis* have been studied more extensively in subsequent studies (Chinsamy et al., 2020; Gao et al., 2012; Prondvai et al., 2018; Zheng et al., 2014).

The first Jehol enantiornithine to be studied osteohistologically was the bohaiornithid *Zhouornis* (Zhang et al., 2013). Since 2013 there has been a surge of data regarding the histology of stem birds as numerous specimens from the rich Jehol Biota have been sectioned and studied (Bailleul et al., 2019b; Hu and O'Connor, 2017; O'Connor et al., 2014; O'Connor et al., 2015a; O'Connor et al., 2018; Wang et al., 2017a; Wang et al., 2017b; Wang et al., 2018; Wang et al., 2016; Wang and Zhou, 2016; Zheng et al., 2014). Most of these studies are descriptions of new taxa, with the histological analysis conducted primarily to offer support in favor of interpretations that the individuals being used for the basis of holotypes were adults or subadults and could thus be expected to change minimally with advancing ontogeny. However, more recently histology has been used to investigate other aspects of stem avian biology such as biomechanics, reproduction, and physiology (Bailleul et al., 2019a; Cubo et al., 2022; O'Connor et al., 2018; Wang et al., 2020; Wu et al., 2021). New histological studies of stem birds from outside China have been far less frequent, although recently the most complete enantiornithine from North America *Mirarce eatoni* (Atterholt et al., 2018) was sampled extensively revealing a complex growth history (Atterholt et al., 2021).

The Enantiornithes are the dominant clade of Cretaceous land birds and account for approximately half of all avian diversity during this period (O'Connor et al., 2011; Wang and Zhou, 2017). Not surprisingly, this clade includes the largest number of species that have been examined histologically (Cabra-Moo et al., 2006; Chinsamy et al., 1994; Chinsamy and Elzanowski, 2001; Cubo et al., 2022; Hu and O'Connor, 2017; Hu et al., 2015; O'Connor et al., 2014; O'Connor et al., 2018; Wang et al., 2017a; Wang et al., 2017b; Wang et al., 2020; Wang et al., 2014). More than half of all known species are from the Early Cretaceous Jehol Biota in northeastern China (O'Connor et al., 2011; Wang and Zhou, 2017). The avian bearing sediments are dated between 130 and 120 Ma (Pan et al., 2013; Yang et al., 2020). Up until now, histologically sampled Jehol enantiornithines consisted primarily of specimens regarded as subadults and adults. These specimens reveal thin cortices with minimal vascularization and variably have one or two growth lines present (Table 1). An inner circumferential layer (ICL) is typically present but rarely a distinct outer circumferential layer (OCL).

Both the absence of available growth series and the limited understanding of ontogenetic changes in bone tissue in stem avians hinders interpretations of sectioned specimens and inferences regarding relative maturity. Adult and embryonic enantiornithines were among the earliest stem-birds studied histologically but these come from much younger deposits, separated from the abundant histological data from Jehol specimens by over 50 myr (Chinsamy et al., 1994; Chinsamy and Elzanowski, 2001). A late-stage embryo referred to *Gobipteryx* from the Late Cretaceous of Mongolia reveals a taxon that grew rapidly during embryological development, depositing woven bone with large vascular spaces which the authors described as fibrolamellar (Chinsamy and Elzanowski, 2001). Rapidly formed bone is characteristic of the embryological growth of almost all living animals (Horner et al., 2001). Traces of this embryological growth are completely lost over the course post-hatching ontogeny, as in living birds (Atterholt and Woodward, 2021).

Two femora from the Late Cretaceous Lecho Fm. in Argentina reveal avascular parallel fibered bone marked by four to five well-spaced LAGs, indicating that at least some enantiornithines

Table 1
Comparison of cortical thickness in juvenile enantiornithines and *Mirusavis* IVPV V18692.

Specimen number	Ontogenetic stage	Humeral length (mm)	Femoral length (mm)	Element	Cortical thickness (µm)	Average thickness (µm)	Cortical thickness: bone length	Average vascular canal area (µm ²)	Reference
ZPAL MgR-190	Embryo	–	–	tibia	282–382	332			Chinsamy and Elzanowski (2001)
IVPP V15575	Early immature	15.7	13.7	humerus	68–110	89	0.176	172	This study
IVPP V15686	Early immature	17	15.6	tibia	57–139	98		320	This study
MPCM-LH-26189	Early immature	10.6	10.8	tibia	56–137	96.5		489	This study
				radius	54–82	68			Knoll et al. (2018)
				tibia	60–80	70		159	Knoll et al. (2018)
IVPP V18586	Late immature	18.4	14.5	humerus	126–159	142.5	0.129		Wang et al. (2014)
IVPP V21711	Late immature?	19.35	19.75	humerus	97–139	118	0.164		Wang et al. (2017a, 2017b)
IVPP V16892	Mature	30	27.3	humerus	167–246	206.5	0.145		Wang et al. (2020)
				radius	139–203	171			Wang et al. (2020)
				femur	204–241	222.5	0.123		Wang et al. (2020)
				tibiotarsus	183–266	224.5			Wang et al. (2020)

grew slowly for at least the last four-five years of their lives (Chinsamy et al., 1994, 1995). The histology of *Mirarce* from the Late Cretaceous Kaiparowits Fm. in Utah reveals a more complex growth history, involving periodic rapid growth interrupted by the formation of LAGs, in which incipient fibrolamellar bone *sensu* Woodward et al. (2014) was deposited in the humerus during the rapid growth phase, followed by a distinct OCL containing at least four closely spaced LAGs (Atterholt et al., 2021). This appears to be a more determinate growth strategy compared to the Lecho enantiornithines. In sampled Jehol enantiornithines, the absence of a distinct outer layer of parallel fibered bone tissue and presence of fewer LAGs compared to these Late Cretaceous adult enantiornithines may suggest most previously sampled Jehol individuals are not fully mature and that an OCL, possibly with additional LAGs, would have formed if growth had not been truncated by death. Alternatively, these differences reflect true variations in growth strategy.

The currently available data does not lend itself to clear interpretations regarding the growth strategy of enantiornithines or the changes in tissue formation that occur during different ontogenetic periods. This may at least be partially attributed to the specific diversity of this large clade, which likely evolved varied growth strategies during their 64 myr documented evolutionary history (Atterholt et al., 2021). However, major gaps in our understanding hinder ontogenetic interpretations. For example, until this study the histology of post-hatching early immature individuals was unknown, and it remains unclear if specimens without LAGs reached adult size within a year, if LAGs were lost through resorption due to medullary expansion, or if growth never slows enough to form LAGs.

Eleven 'juvenile' enantiornithines have been reported previously from the Jehol deposits (Chiappe et al., 2007; Hou and Chen, 1999; Ji and Ji, 1999; Wang et al., 2021; Zheng et al., 2012). Although most of these specimens are largely complete, the skeleton is typically recorded only as an impression (e.g., IVPP V15664, GMV-2156) or void (e.g., GMV-2159), or the bone is poorly preserved (e.g., STM34-1). Recently two new juvenile enantiornithine specimens (IVPP V15686 and V15575) with much of the bone preserved intact were identified at the Institute of Vertebrate Paleontology and Paleoanthropology (Figs. 1, 2). They are regarded as ontogenetically immature based on the incomplete ossification of the sternum (Zheng et al., 2012), absence of fusion in certain compound elements (e.g., the carpometacarpus, tibiotarsus, tarsometatarsus, pygostyle; Hu and O'Connor, 2017), and the heavily striated and pitted surfaces of the bones (Tumarkin-Deratzian et al., 2006) (Fig. 3). These specimens also preserve pre-existing breaks that could be utilized for histological sampling with minimal damage.

We describe the bone histology of these two specimens and discuss the implications of this data with regard to our understanding of enantiornithine growth strategies and the differences in bone deposition that characterize the early ontogeny of this diverse clade. Hu and O'Connor (2017) attempted to correlate skeletal development in enantiornithines with histological data, focusing on the sequence in which major compound elements (e.g., synsacrum, pygostyle, carpometacarpus) become fused (Hu and O'Connor, 2017). This study was also hindered by the absence of histological data concerning post-hatching juveniles available at the time. Although several juveniles have been reported, most have not been fully described, limiting attempts to understand ontogenetic transformations. In order to explore early ontogenetic skeletal changes in enantiornithines we also describe the skeletal morphology of these two specimens and expand on the table put forth by Hu and O'Connor (2017) relating the sequence of skeletal fusions to osteohistology.

2. Material and methods

IVPP V15575 and V15686 are deposited in the Institute of Vertebrate Paleontology and Paleoanthropology of the Chinese Academy of Sciences in Beijing, China (IVPP). Both specimens are from the 120 Ma Jiufotang Fm., the youngest stage in the Jehol Biota (Pan et al., 2013). IVPP V15575 was collected from the Damiao locality near Chifeng City, Songshan District, in Inner Mongolia. IVPP V15686 was found at the Lamadong locality in Jianchang County, Liaoning Province. Bone samples were extracted with a rotating tool equipped with a diamond blade (Dremel 8100). Subsequently, the fragments were prepared using the paleohistological ground-sectioning technique: Samples were embedded in EXAKT Technovit 7200 (Norderstedt, Germany) one-component resin, and cured for 24 h, cut using an EXAKT 300CP accurate circular saw, and then ground and polished using the EXAKT 400CS grinding system (Norderstedt, Germany) until the desired optical contrast was reached (between 20 and 30 μm). Sections were observed under both natural and polarized light using a ZEISS AX10 light microscope (Thornwood, USA). Photographs were taken using the camera ZEISS AxioCam MRC5 (Thornwood, USA) and the software Axio Vision SE64 (Rel. 4.9).

Average cortical thickness was calculated by averaging the lowest measured cortical thickness with the greatest measured cortical thickness. However, in many specimens incomplete preservation of the bone cortex or breakage means that these values may not reflect the true variation of the bone wall.

Thin sections of extant crown birds are taken from the dataset published in Atterholt and Woodward (2021); please refer to this publication for details on specimen origin and preparation. Scans of the *Megapodius pritchardi* hatchling (UMZC 14.Meg.6.g.1) were produced using the Nikon XTEK H 225 ST MicroCT scanner housed at the Cambridge Biotomography Centre with a voxel size of 28.931 μm .

Institutional abbreviations: GMV, Geological Museum of China, Beijing, China; IVPP, Institute of Vertebrate Paleontology and Paleoanthropology, Beijing, China; MPCM, Museo de Paleontología de Castilla-La Mancha, Cuenca, Spain; MVZ, Museum of Vertebrate Zoology, University of California, Berkeley, United States of America; PIN, Paleontological Institute, Moscow, Russia; STM, Shandong Tianyu Museum of Nature, Pingyi, China; UMZC, Museum of Zoology, University of Cambridge, Cambridge, United Kingdom; ZPAL, Institute of Paleobiology, Polish Academy of Sciences, Warsaw, Poland.

3. Results

Anatomical nomenclature primarily follows Baumel and Witmer (1993) mostly using the English equivalents of the Latin terminology. The terminology used to qualitatively classify and describe bone tissues follows the precedent of Francillon-Viellet et al. (1990) and de Ricqlès (1976), as updated by Huttenlocker et al. (2013).

3.1. Ontogenetic nomenclature

For descriptive purposes it is necessary to subdivide the ontogenetic continuum into artificial, discrete categories. Previously described immature specimens of enantiornithines have been referred to as 'juveniles' or 'subadults' with little to no information provided regarding what was precisely meant by each of these categories and how they differ with regards to their skeletal morphology and bone tissue beyond the assumption a juvenile is less mature than a subadult. Also problematic with enantiornithines



Fig. 1. Photograph (A) and line drawing (B) of early immature enantiornithine IVPP V15686. Rectangles indicate the right thoracic girdle and forelimb and left pelvic girdle and hindlimb. Anatomical abbreviations: 1–5, phalanges; al, alular metacarpal; ca, caudal vertebrae; ce, cervical vertebrae; co, coracoid; fe, femur; fu, furcula; gs, gastralia; hu, humerus; hy, hypocleidium; il, ilium; is, ischium; ma, major metacarpal; mi, minor metacarpal; pu, pubes; py, pygostyle; ra, radius; ri, ribs; rl, radiale; sa, sacral vertebrae; sc, scapula; sr, sternal rib; st, sternal ossifications; th, thoracic vertebrae; ti, tibia; ul, ulna; un, ulnare. Scale bar: 10 cm.

is the use of ontogenetic terminology for juvenile birds linked to plumage: hatchling, nestling (or pin-feather stage), and fledgling (Sanz et al., 1997; Xing et al., 2017). Fledgling is an ontogenetic stage that is associated with the full development of the remiges and the onset of flight. All known immature enantiornithine material represent individuals with highly precocial developmental strategies that hatched fledged (thus in this case, hatchlings are

also fledglings; Xing et al., 2017; Zhou and Zhang, 2004), which among extant birds occurs only in the Megapodiidae (Stark and Ricklefs, 1998).

To clarify discussions of enantiornithine development it is necessary to more precisely define ontogenetic terminology moving forward. It has recently been suggested that vague categories such as ‘juvenile’ and ‘subadult’ should be abandoned in favor of more

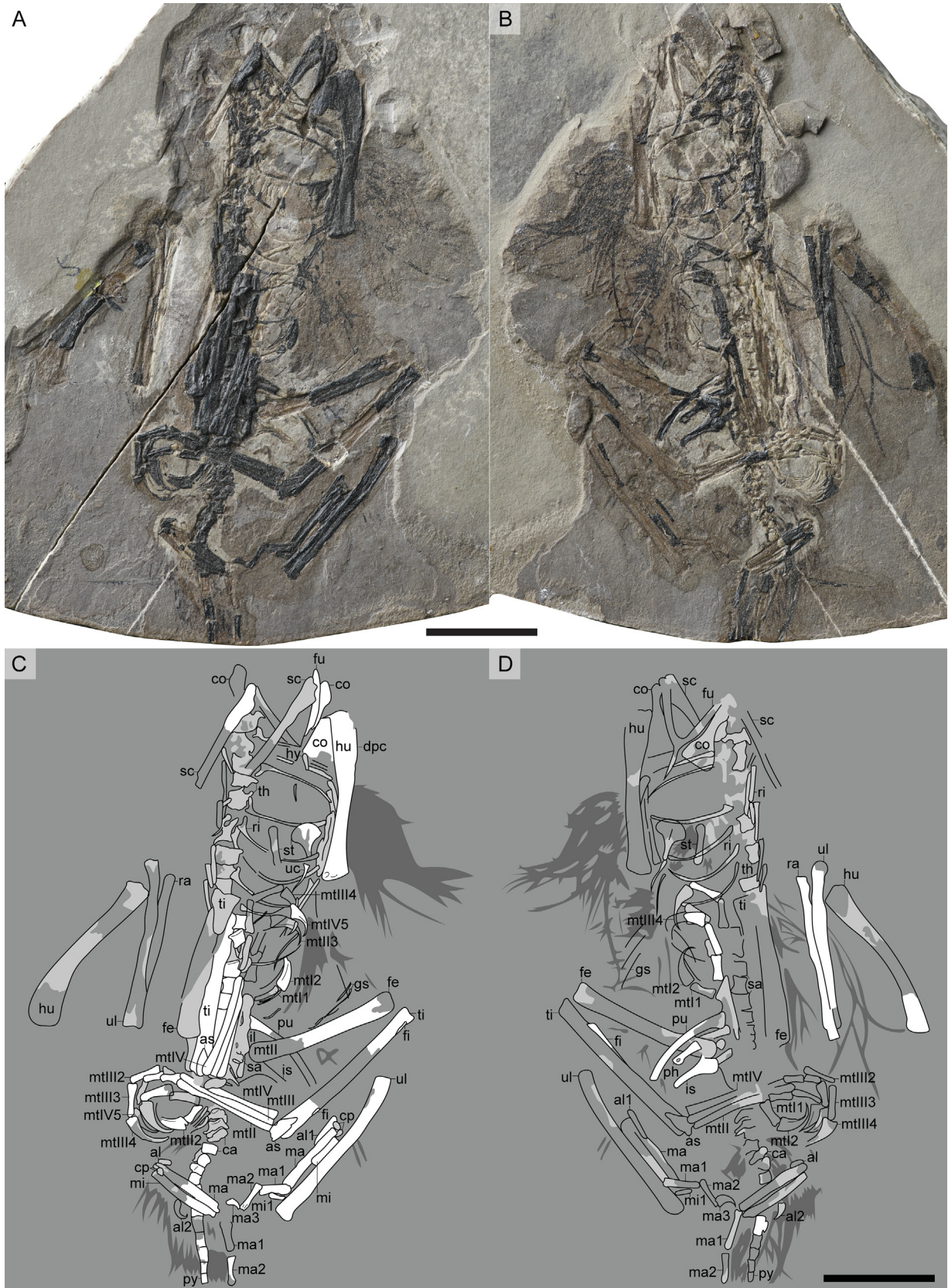


Fig. 2. Photographs (A, B) and line drawing (C, D) of early immature enantiornithine IVPP V15575 preserved in a main slab (A, C) and counter slab (B, D). Anatomical abbreviations not listed in Fig. 1 caption: as, astragalus; cp, free carpal; dpc, deltopectoral crest; mtlI-IV, metatarsals; ph, phalanx. Scale bar: 10 cm.

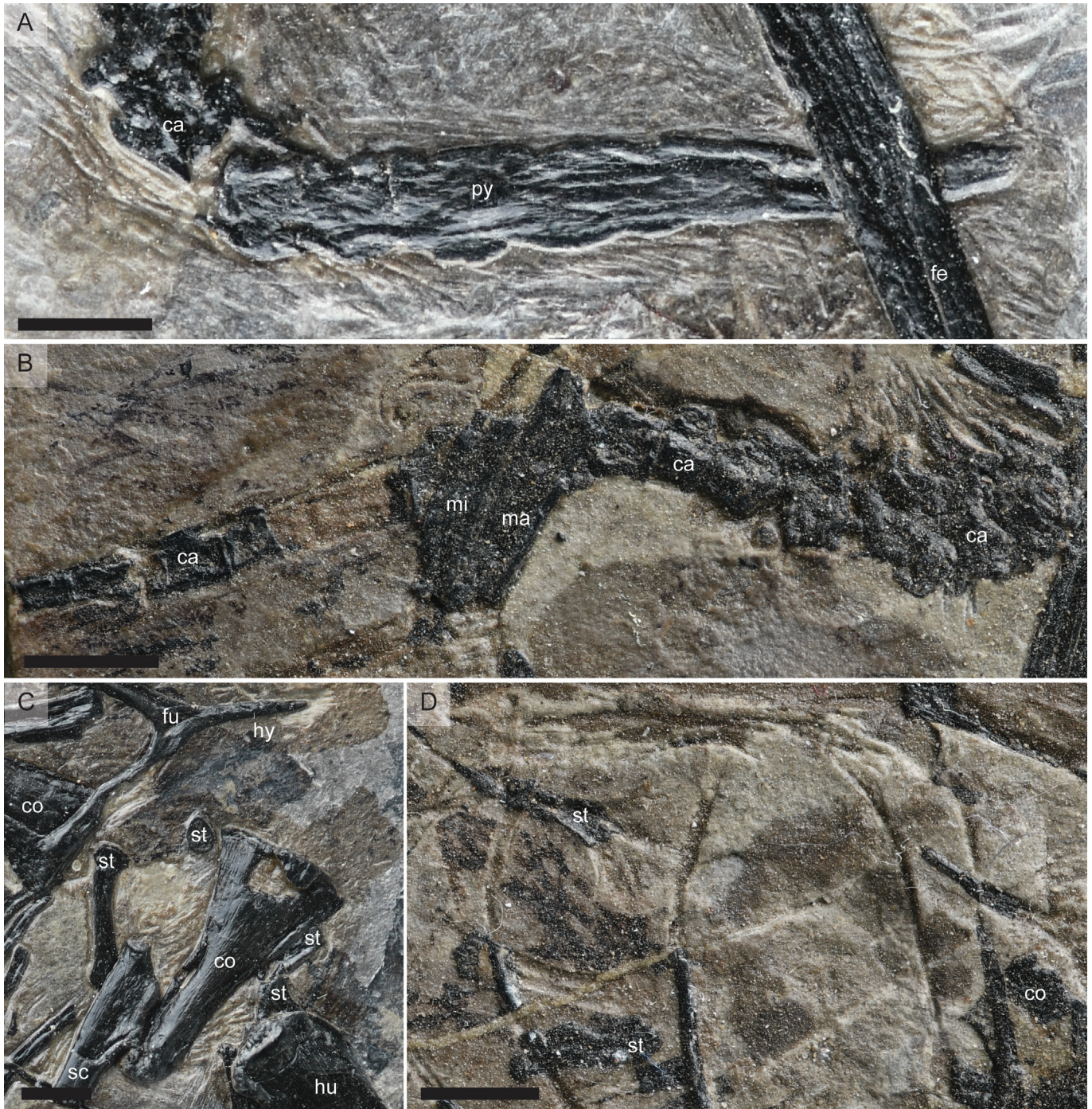


Fig. 3. Close up of well-preserved unfused compound elements supporting identifications of early immaturity. **A.** Pygostyle, IVPP V15686. **B.** Pygostyle, IVPP V15575. **C.** Sternum, IVPP V15686. **D.** Sternum, IVPP V15575.

specific and intentional terminology (Griffin et al., 2021). Griffin et al. (2021) also make the necessary point that the various metrics used to determine maturity (e.g., skeletal fusion, body size, osteohistology) need to be assessed and described separately. Following Griffin et al. (2021), we use the terminology morphologically immature/mature to refer to the development of the skeletal gross anatomy. We use osteohistologically immature/mature to refer to the ontogenetic characteristics of the bone tissue.

Griffin et al. (2021) additionally suggests that data permitting, immature specimens can be further into ‘early’ and ‘late immature.’ For this to be useful, it is necessary to define what differen-

tiates an early vs. late immature enantiornithine at both the morphological and osteohistological level. Morphologically early immature is here defined as the complete absence of fusion between the four sternal anlagen and incomplete ossification of the pygostyle or a proportionately elongate pygostyle; morphologically late immature is defined as having fully fused sternal anlagen but lacking fusion between the semi-lunate carpal and the major and minor metacarpals, proximal tarsals and the tibia, and the distal tarsals and the proximal metatarsals. Osteohistologically early immature is defined as a complete lack of ICL and OCL in combination with a relatively high porosity; histologically late immature is

defined as the presence of an ICL but without clear signs that periosteal growth is slowing. The definitions provided here for these ontogenetic stages represent an initial attempt that will be refined as new data becomes available.

3.2. Morphological descriptions

3.2.1. IVPP V15686

This specimen consists of a small (humeral length of 17 mm; femoral length of 15.9 mm), partially articulated enantiornithine missing only the skull, cranial-most cervical vertebrae, and hind limb elements distal to the femora (Fig. 1). The caudal half of the skeleton is separated from the cranial half and preserved a slight distance away, with thoracic ribs and gastralia scattered between them. It is identified as enantiornithine based on the presence of an elongate hypocleidium on the furcula such that this element is Y-shaped, a straight and strap-like scapular corpus, and a minor metacarpal projecting farther distally than the major metacarpal (Chiappe and Walker, 2002; O'Connor et al., 2011). It is considered to be morphologically early immature based on the partially ossified sternum in which the cranial midline ossification is small and does not approach the caudal midline ossification (Zheng et al., 2012), absence of fusion between the distal carpals and the metacarpals (Chiappe et al., 2007), the simple morphology of the humeral epiphyses, the incomplete fusion of the sacral vertebrae (Hu and O'Connor, 2017), and the elongate morphology of the pygostyle (Chiappe et al., 2007). The bone is preserved black and heavily compressed such that the bones are nearly flat. Striations are visible on the bone surface indicating periosteal ossification was incomplete at the time of death (Fig. 1).

Four complete, caudal cervical vertebrae are preserved in articulation and dorsally exposed on one side of a crack that runs through the skeleton, interrupting a fifth preserved vertebra, at approximately the level of the cervicothoracic transition. The cervical vertebrae overlie the left humerus. They are much wider than long, as observed in GMV-2158 (Chiappe et al., 2007). The prezygapophyses are cranio-laterally oriented and represent the widest point of the vertebrae. The postzygapophyses are caudally oriented, whereas they are caudolaterally oriented in GMV-2158 (Chiappe et al., 2007).

Caudal to the crack there are thirteen additional articulated presacral vertebrae. A fourteenth may be overlain by the left ulna. The first four appear to be primarily in dorsal view and the first two may be cervicothoracics with thoracic ribs pushed cranially so that they appear to articulate with these vertebrae. The following nine vertebrae are thoracics (dorsals) preserved in right lateral view, revealing tall (dorsoventral length exceeds craniocaudal length) neural spines with concave caudal margins; the neural spines appear proportionately shorter and more craniocaudally elongated in GMV-2158 (Chiappe et al., 2007). The postzygapophyses are larger than the prezygapophyses and project strongly beyond the caudal margin of the spool-shaped centra.

In the displaced caudal half of the skeleton, there are 17 articulated vertebrae cranial to the pygostyle. The first is interpreted as a thoracic. The following eight are interpreted as sacral vertebrae. They are proportionately wider and shorter than the thoracic vertebrae. As in other morphologically early immature enantiornithines (Chiappe et al., 2007), the sacrals are unfused although it is possible there is some degree of incipient fusion between the distal three vertebrae, in which clear spaces are not visible between the centra. The transverse processes are laterally oriented in the penultimate sacral and caudolaterally in the last sacral, also commonly observed in more mature enantiornithines (e.g., *Rapaxavis*, *Sulcavis*, *Pengornis*).

Typical of enantiornithines there are eight free caudal vertebrae, which decrease in size distally. Prezygapophyses are well

developed, measuring nearly half the craniocaudal length of their associated centra. Transverse processes are clearly visible in the cranial five caudal vertebrae; they are approximately two-thirds the mediolateral width of their centra and caudolaterally oriented.

The pygostyle is long and tapered, with a blunt distal margin. The first two incorporated vertebrae are incompletely fused (Fig. 3(A)). The caudal-most vertebrae of the pygostyle are also unfused. We estimate that there are three unfused distal vertebrae; the exact number is obscured by overlap with the femur. The proximal two incompletely fused vertebrae of the pygostyle are nearly square, slightly longer than wide. The ventral surface of these vertebrae preserve haemal arches that are approximately as long as their associated vertebrae. They are tapered proximally and distally with convex ventral margins. Along the dorsal side of the incipient pygostyle there is a thin layer of incompletely fused structures that are interpreted as the incompletely fused neural spines and zygapophyses.

The cranial thoracic ribs are grooved on their ventral surfaces, probably for the intercostal neurovascular bundle. The first three right thoracic ribs are proximally still in near articulation with the thoracic vertebrae but they have been rotated laterally and caudally so that the shaft of the ribs are aligned in parallel with the axial column. The vertebrae tentatively identified as the fourth through eighth thoracics preserve the right thoracic ribs in articulation, revealing their proximal ends bifurcated into a shorter tuberculum and a longer capitulum. The distal end of the tentative fourth through seventh thoracic vertebral ribs are strongly expanded distally (more than double their mid-length width) for articulation with sternal ribs, which are preserved in articulation with the cranial two of these ribs.

Five disarticulated thoracic ribs are preserved cranial to the caudal half of the skeleton. These are nearly twice as long as the thoracic ribs articulating with the sternal ribs. Their distal ends are also expanded to more than twice their midshaft width. A short fragment preserved appressed to one of the ribs may be an uncinatous process. Seven gastralia are preserved near the cranial sacral vertebrae. Two of the gastralia consist of lateral and medial rods in articulation. The medial end of the medial rod forms a rounded expansion, as in mature enantiornithines (O'Connor et al., 2015b).

Both coracoids are preserved in ventral aspect. The coracoids are strut-like; the omal half is narrow and the sternal half forms a fan-shaped expansion ending in a straight sternal margin. On the right the ventral surface is gently convex and heavily striated, especially towards the sternal margin. The supracoracoidal nerve foramen, visible on both coracoids, is omal-sternally elongate and separated from the medial margin by a thin bony bar. A procoracoid process is absent. The medial margin is gently concave; the lateral margin is nearly straight. The sterno-medial corner is slightly expanded forming a weak angulus medialis.

The right scapula is laterally exposed and nearly complete although the midshaft is preserved as a void. Only the distal portion of the left scapula is preserved. The shaft is straight and the distal end is blunt, only slightly narrower than the midshaft. The acromion process is short, approximately half the length of the glenoid surface. The exposed lateral margin of the glenoid is expanded forming a labrum.

The elongate hypocleidium of the ventrally exposed furcula (clavicula) appears to be distally complete, tapering bluntly. The omal ends of the rami are not preserved. As preserved the hypocleidium is half the length of the more complete ramus. The furcular rami define a 65° angle.

The sternum is incompletely ossified, as in other early immature enantiornithines (Zheng et al., 2012). All four sternal anlagen are preserved. Both bilateral ossifications and the caudal midline ossification are partially covered by the right coracoid and humerus (Fig. 3(I)). A distinct sternal keel does not appear exposed

on the caudal midline ossification indicating the sternal anlagen as exposed in dorsal aspect. The lateral ossification is strap-like and weakly expanded at both ends. The cranial midline ossification is small and lacrimiform, with the tapered end rostrally oriented, whereas the tapered end is caudally oriented in STM34-9 and STM34-1 (Zheng et al., 2012); it is uncertain if this is a true difference or a preservational artifact. As in all known early immature enantiornithines, the caudal midline ossification is fan shaped cranially, where it contributes to the sternal body, with the caudal half forming the strap-like xiphoid process.

Both humeri are preserved in caudal view. The proximocaudal margin is convex as in other enantiornithines. The proximal margin appears broadly convex on the right humerus, but the saddle shape characteristic of enantiornithines is weakly developed on the left. The articular surface is not separated from the ventral tubercle by a capital groove. The deltopectoral crest is very weakly developed and narrow so that the proximal end of the humerus is only slightly wider than the distal end. The narrowest point of the element is just below the deltopectoral crest, distal to which the shaft becomes wider. The distal end is weakly angled relative to the long axis of the shaft as in many enantiornithines (Chiappe and Walker, 2002). The ulna is only slightly narrower than the narrowest point of the humerus but this may be exaggerated by compaction. It is proximally bowed as in other enantiornithines. The radius is straight and two-thirds the width of the ulna.

Both hands are complete except for their distal extremities. Identification of preserved carpals is complicated by slight disarticulation, differences in preserved view, and the early ontogenetic stage of the specimen. The right hand preserves two visible free carpals. One is very small and appressed to the major metacarpal; this is tentatively identified as the semilunate carpal. Its true size may be obscured by the radius. The other free carpal is approximately four times its size and is probably the pisiform (ulnare). The left preserves three or four free carpals. The existence of the fourth carpal, a possible carpal x (or distal carpal three; Botelho et al., 2014) articulating with the proximal end of the minor metacarpal (Chiappe et al., 2007), is equivocal due to preservation. If it is present on the left, it is already fused to the minor metacarpal on the right, as the major and minor metacarpals clearly begin at the same level. The carpal on the left that articulates with the proximal end of the major metacarpal, tentatively identified as the semilunate, is much larger than that on the right. A small carpal with a round profile is preserved contacting the semilunate carpal and tentatively identified as the scapholunare (radiale). Another carpal, tentatively identified as the pisiform, is preserved exposed between the proximal end of the minor metacarpal (or distal carpal three) and the ulna, slightly overlapped by both bones.

The metacarpals are ventrocaudally exposed on the right and dorsally exposed on the left. The major metacarpal is thicker than the minor metacarpal and straight, as in other enantiornithines. The minor metacarpal is slightly bowed creating a small intermetacarpal space (visible on the left manus). On both sides the minor metacarpal extends distally much farther than the major metacarpal, a synapomorphy of Enantiornithes (O'Connor et al., 2011). The alular metacarpal is best preserved on the right manus. It articulates with a short digit that consists of two phalanges and would not have extended to the distal margin of the major metacarpal. The proximal phalanx of the major digit is longer than the penultimate phalanx. The phalanges are narrower than the major metacarpal and taper distally. A single minor digit phalanx is preserved on both sides. It is long and narrow, tapering distally.

The pelvic girdle is completely unfused. The left ilium is medially exposed; the right is in lateral view. The preacetabular wing is only about 5% longer than the postacetabular wing but nearly twice its dorsoventral height. The postacetabular wing is described as 25% shorter than the preacetabular wing in GMV-2158 and

–2156 although the ilia are not clearly preserved in either specimen (Chiappe et al., 2007). The rostral margin is sharply convex. The dorsal margin is weakly convex. As in other enantiornithines, the pubic pedicel is longer and wider than the ischiadic pedicel and the margin between the two demarcates the dorsal margin of the acetabulum. The ischiadic pedicel bears a laterally directed eminence that is interpreted as the antitrochanter. The postacetabular wing is deflected slightly ventrally. The distal end is untapered and ends abruptly with a blunt, convex distal margin.

The pubes are bowed such that the cranial margin is convex and the caudal margin is weakly concave. They are weakly expanded at the proximal and distal ends. The ischium is 2/3 the length of the pubis and tri-radiate with a cranial process weakly bifurcated into the articular surfaces of the ilium and pubes, a craniodorsally oriented dorsal process typical of enantiornithines, and the ischiadic blade, which is the longest and narrowest of the processes. The medial surface is grooved although this may be an artifact of compaction. Distally, the blade does not taper. The dorsal process is well developed and may have contacted the ilium.

The femur is long and straight. The femoral head is weakly developed and not separated from the shaft by a distinct neck. The posterior trochanter does not appear to be developed. Only a small portion of the right tibia is preserved. The articular surface is rounded in profile which may suggest it is the distal and not the proximal end, despite its proximity to the femur.

3.2.2. IVPP V15575A/B

This small (humeral length of 15.7 mm; femoral length of 13.7 mm), partially articulated enantiornithine is nearly complete, missing only the skull and cervical vertebrae and the left manus (Fig. 2). It is preserved in a slab and counterslab with traces of feathers mostly located in the counterslab (IVPP V15575B) and around the cranial half of the skeleton. The skeleton is heavily compressed. It can be identified as enantiornithine based on the straight scapula and Y shaped furcula (Chiappe and Walker, 2002; O'Connor et al., 2011). It is identified as an early immature individual based on the absence of fusion between the distal carpals and the metacarpals, the simple morphology of the humeral epiphyses, and the incomplete fusion of the sacral vertebrae, pygostyle, and sternum (Chiappe et al., 2007; Fig. 3).

The cranial thoracic vertebrae are poorly preserved, torn between the two slabs. We estimate a total of 11 thoracic vertebrae based on the number of thoracic ribs. The sacral vertebrae appear unfused but they are mostly covered by the right hindlimb, which is folded below the pelvis. At least 15 articulated vertebrae emerge caudal to the pelvis, proximally overlain by the left metatarsals. The proximal-most of these vertebrae are short and wide. The distal vertebrae are more elongated being longer than wide. It appears that the vertebrae have not yet begun to coalesce into a pygostyle or are only in the very early stages of doing so. In other known early immature enantiornithines at least some fusion is observed between the caudal vertebrae that will form the pygostyle (Chiappe et al., 2007; Wang et al., 2021) although the complete absence of caudal fusion is observed in an immature specimen of the basal ornithuromorph *Archaeorhynchus* IVPP V17075 (Zhou et al., 2013). The caudal series is truncated by the slab.

The left thoracic ribs are curved and decrease in length and robustness caudally. The right thoracic ribs appear to be preserved so that they are parallel to the right lateral margin of the thoracic vertebrae. A few short elements, expanded with a flat margin at one end and tapered at the other, are interpreted as uncinat processes. They appear proportionately long compared to those observed in adult enantiornithines. A few gastralia are also preserved rostral to the pelvis.

The thoracic girdle is ventrally exposed. The coracoid is strut-like: elongate, narrow at the omal end, and expanded towards

the sternal margin. The ventral surface near the sternal margin is heavily marked by striations indicating active growth.

The omal portions of both scapulae are preserved in articulation with the coracoids and furcula. The scapulae appear to have poorly developed acromion processes that are short and blunt, approximately equal in cranio-caudal and dorsoventral length. The scapular blade is straight and untapered.

The furcula is somewhat distorted but it appears slightly more narrow than that of IVPP V15686; we estimate the angle was between 53° and 62°. The hypocleidium is elongate and tapers distally. A small, delicate, sharply tapered fragment in the main slab may be the distal third of the hypocleidium. If correct, it has also been displaced for it is not in line with the remainder of the hypocleidium. Alternatively, this may represent part of the cranial midline ossification of the sternum, consistent with its position. As preserved, not including the possible distal fragment, the hypocleidium measures half the length of the furcular rami.

Two sternal ossifications are definitively preserved: the caudal midline ossification center forming the xiphoid process and the right bi-lateral ossification that forms the right lateral trabecula (Fig. 3(D)). The rostral half of the caudal midline ossification is fan-shaped, as in other early immature enantiornithines (Zheng et al., 2012). The lateral ossification is fairly robust, being wider than the xiphoid process but not as proportionately wide as in STM34-2 (Zheng et al., 2012), and weakly expanded at the rostral and caudal ends.

The left humerus is cranially exposed and preserved just distal to the glenoid formed by the scapula and coracoid. The right is caudally exposed in the main slab and disarticulated, preserved near the right hindlimb. The proximal end of the humerus is heavily striated. The deltopectoral crest is weakly developed and gently tapers into the shaft distally. The humerus is narrowest near its mid-point, after which it widens distally. The distal margin is angled so that the ventral corner is located distal to the dorsal corner. The weakly developed humeral condyles are located on the cranial surface. The ventral condyle is larger than the dorsal condyle.

The right ulna and radius are preserved in near articulation with the displaced humerus. The left ulna is preserved displaced distal to the left hindlimb and the left radius does not appear to be preserved at all. Typical of Mesozoic birds, the ulna is proximally bowed and the radius is straight and narrower than the ulna.

The 'carpometacarpus' is poorly preserved on both sides. The left metacarpals are preserved up against the left ulna. The right metacarpals have drifted away from the proximal forelimb elements and are overlying the caudal vertebrae. Two small, subequal, and subrounded carpals are preserved near the proximal ends of the major and minor metacarpals on both sides. The element that is articulated with the proximal margin of the major metacarpal is probably the semilunate carpal.

The alular metacarpal is preserved on the right and appears to be rectangular and 20% the length of the major metacarpal. On both sides the proximal end of the minor metacarpal is staggered so that it is distal to that of the major metacarpal suggesting the presence of an unossified or simply not preserved distal carpal three. The major metacarpal is straight and more robust than the minor metacarpal. The right minor metacarpal is very weakly bowed. The first phalanx of the alular digit, preserved on the left, is less than half the length of the major metacarpal. The unguis phalanx, preserved on the right, is larger and more recurved than that of the major digit. The major digit consists of three phalanges: the first two are subequal in length, followed by a weakly curved unguis. The first phalanx is slightly narrower than the major metacarpal; the second is more delicate. A single minor digit phalanx is preserved on the left.

The pelvis is mostly exposed on the left. The rostral margin of the ilium is blunt and convex. The postacetabular wing is shorter than the preacetabular wing, narrower and untapered. The pubes are weakly bowed so that the cranial margin is convex and longer than the ischium. The ischium is short with an expanded proximal end. The main body or wing of the ischium (ala ischii) is narrow and untapered.

The right leg is folded under the body so that it covers most of the pelvis. The left leg is mostly preserved to the left of the pelvis, but in such a way that the foot crosses over the caudal vertebrae just caudal to the pelvis. The femur is shorter than the tibia. The astragalus is unfused to the tibia, preserving a tall ascending process visible on both sides. The distal tarsals and metatarsals are unfused. Metatarsals II and III appear to be similar in width and length, with metatarsal III only slightly longer than II. It appears that metatarsal IV was shorter than II but similar in width as in GMV-2158 (Chiappe et al., 2007), whereas this metatarsal is very slender in some mature enantiornithines (O'Connor et al., 2011) but certainly not all (e.g., *Qiliania*, *Feitianius*). The third pedal digit is the longest. The pedal phalanges become longer distal within each digit. The pedal claws are large and recurved.

Feathers are preserved on the left side of the body below the shoulder and cranial to the hindlimb. Some feathers are also preserved on the right at the level of the displaced forelimb and surrounding the caudal vertebrae. Most of the preserved feathers are long and narrow without clear subdivision between rachis and vane, resembling immature (growing) feathers identified in several early immature enantiornithines and the holotype of *Crualis pennia multidonta* (O'Connor et al., 2020).

3.3. Histological descriptions

3.3.1. Interpretation of the slides

The tibial sections from both specimens require a section to justify interpretations of the observed bone tissue. Superficially the bone fragment extracted from IVPP V15686, and to a lesser degree IVPP V15575, appears to consist of only a portion of the cortex recording roughly half of the tibial cross-section (Figs. 4, 5). However, we interpret that the entire cross-section of the bone is preserved but that the medullary cavity has been collapsed by post-mortem compression, consistent with the fact the bone walls in these very small, early immature individuals are very thin and the skeletons are very two-dimensionally preserved (Figs. 1, 2). This interpretation is supported by comparison of the cortical thickness with other early immature and mature enantiornithines (Table 1).

In IVPP V15686 the entire preserved bone sample measures between 158 and 239 µm thick; the surface that contacts the matrix is scalloped while the opposite surface is smooth and there is no obvious misalignment between large vascular canals along breaks, thus appearing to represent a partial section of the tibial cortex (Fig. 4). Measured in its entirety, the sample of IVPP V15575 ranges between of 146.6 and 236.2 µm. However, in the interpretation that the entire cross-section of the tibia is preserved and the medullary cavity is collapsed except for one small remnant visible towards the left-hand side of the sample (Fig. 5), the preserved cortical bone thickness of IVPP V15575 measures between of 57 and 139 µm. This value is closer to that of the humeral sample taken from the same specimen, which clearly represents only one half of the diaphyseal cross section and has a thickness ranging from 76 to 110 µm.

Data from MPCM-LH-26189, another similarly sized early immature enantiornithine individual (Table 1), demonstrates that the cortical thicknesses of the forelimb and hindlimb long bone elements in immature enantiornithines are similar. In MPCM-LH-

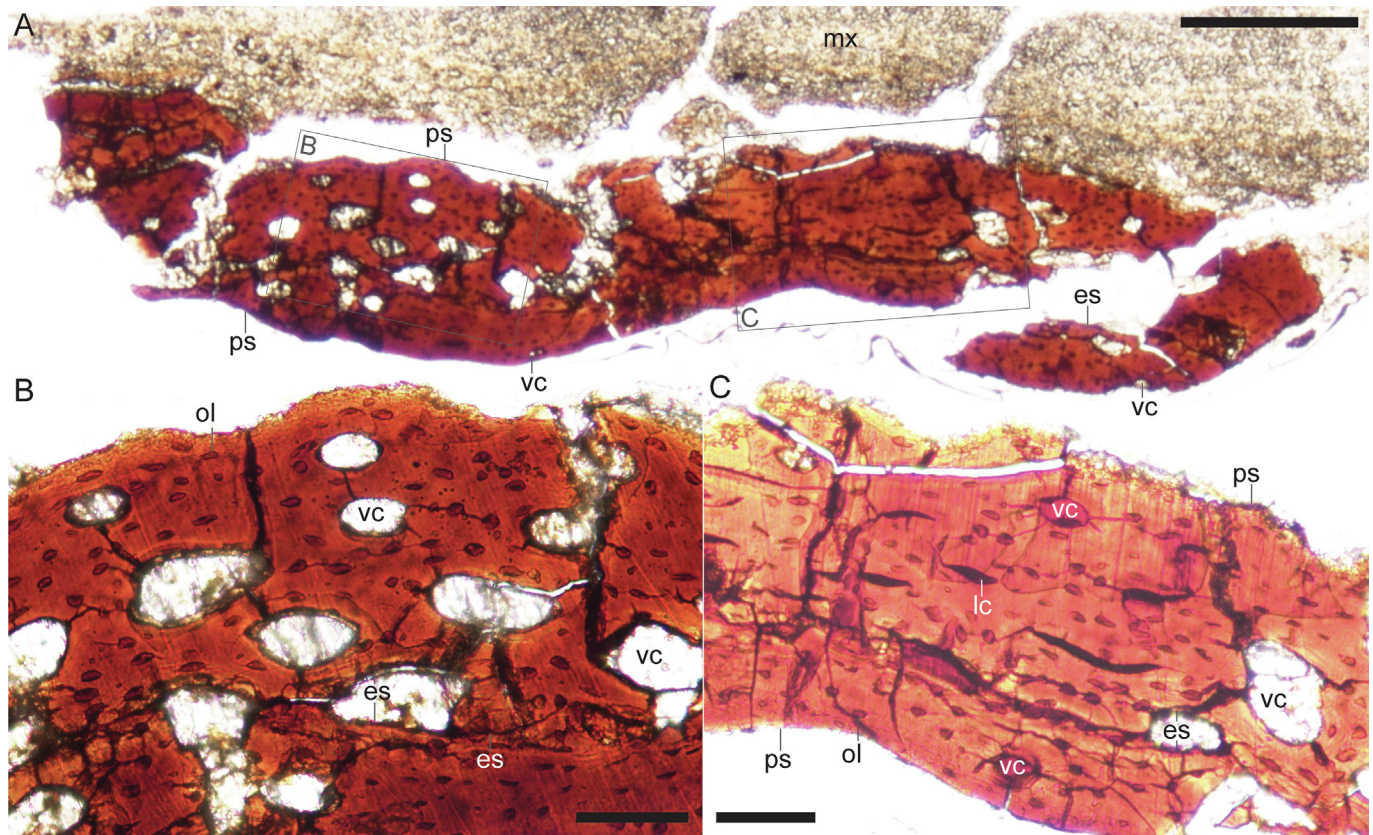


Fig. 4. Osteohistology of the tibia of early immature enantiornithine IVPP V15686. **A.** Entire cross-section. **B, C.** Two regions indicated by rectangles in (A) shown in higher magnification. Anatomical abbreviations: es, endosteal surface; lc, longitudinal canal; mx, matrix; ol, osteocyte lacunae; ps, periosteal surface; vc, large vascular canal. Scale bars: 100 μm (A), 50 μm (B, C).

26189, the cortical thickness of the radius measures approximately 54–82 μm compared to approximately 60–80 μm in the tibia (Knoll et al., 2018). The same pattern is observed in mature enantiornithines. In *Mirusavis* IVPP V18962, the most extensively sampled mature enantiornithine, the cortical thickness of the tibiotarsus measures 183–266 μm (Wang et al., 2020). This range of values largely overlaps with the total thickness of the tibia samples described here if taken at face value (158–239 μm in IVPP V15686; 146.6–236.2 μm in IVPP V15575). However, *Mirusavis* IVPP V18962 is a much larger individual, with a humeral length of 30 mm, nearly twice the length of the immature specimens IVPP V15686 and V15575 investigated here. In *Mirusavis*, the cortical thicknesses of the sectioned forelimb elements also overlap with the range of values observed in the hindlimb elements, as in MPCM-LH-26189 (Table 1).

Together, these data support the interpretation that the bone tissue preserved in the tibial sections in both IVPP V15686 and V15575 represent two sides of the cortex compressed into a single layer. Compaction that blurs the endosteal margins between the two sides of the two dimensionally compressed, collapsed bone cortex is also observed in the radius of MPCM-LH-26189 (Knoll et al., 2018).

3.3.2. IVPP V15686 right tibia

The bone tissue is well preserved in the extracted cortical fragment (extracted sample 1.6 mm wide; Fig. 4). The morphology of the endosteal surface is unclear due to compaction of the bone cross-section. The periosteal surface in contact with the matrix has a weakly scalloped appearance whereas the opposite periosteal surface is smooth. It is unclear to what extent this reflects a gen-

uine textural difference or an artifact of preservation. The cortical thickness measures 56–137 μm . Unfortunately, because the tibia preserves no distinguishing anatomical features it is impossible to determine which surface is embedded in the matrix. The exposed half of the cortex is much thinner than the side embedded in matrix.

The regions of the cortex to the right and left have the highest porosity, consisting of a woven matrix surrounding large (relative to cortical thickness), longitudinally oriented vascular canals (middle sections of both halves of the collapsed cross-section show lower porosity, especially in the thinner half of the cross-section that is not exposed in matrix; Fig. 4(B)). These canals tend to be larger within the thicker region of the cortex. The thinnest parts of the cortex generally show the lowest porosity, as is common in extant hatchlings across the altricial-precocial spectrum (Atterholt and Woodward, 2021). Near the center of the half of the cortex embedded in matrix there is a region of thick cortex with much lower porosity; longitudinal vascular canals are fewer and smaller, some visible as slit-like structures. Uneven porosity is also observed in extant chicks, commonly in precocial chicks but also present chicks across the rest of the altricial-precocial spectrum (Atterholt and Woodward, 2021). These longitudinally-organized canals are oval with their long axis (measuring between 15 and 59 μm) oriented parallel to the periosteal surface.

These highly porous regions of the cortex may suggest that IVPP V15686 died shortly after hatching and that the bone tissue preserved in this specimen formed *in ovo* and has not been absorbed through medullary expansion as in relatively more mature specimens. In the description of *Gobipteryx* ZPAL MgR -/90 these vascular canals are referred to as primary osteons and the bone as

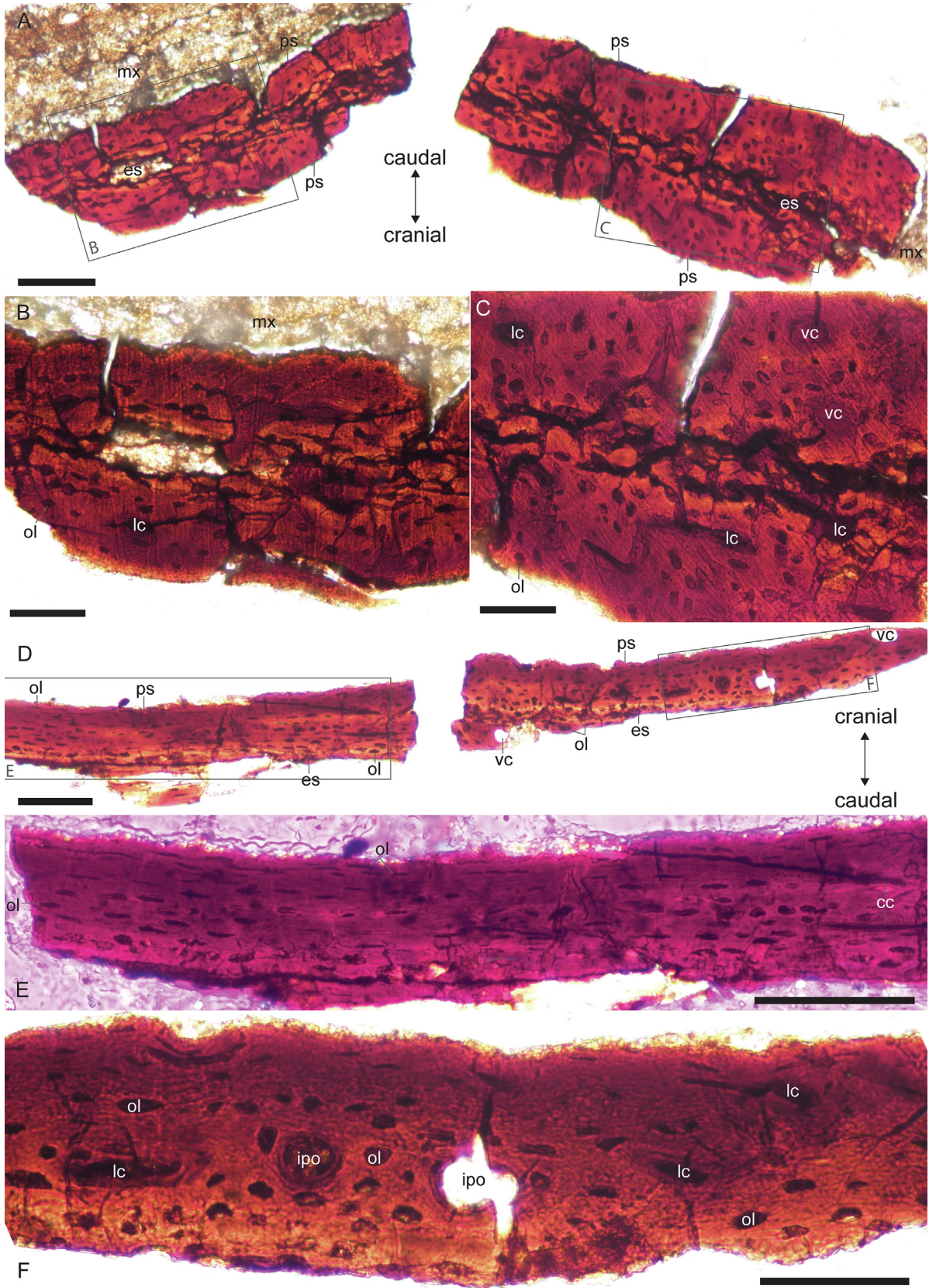


Fig. 5. Osteohistology of early immature enantiornithine IVPP V15575. **A.** Tibia, entire fragment. **B, C.** Close up of regions indicated in (A). **D.** Humeral fragment. **E.** Close up of humeral section indicated in (D) under polarized light. **F.** Close up of region indicated in (D). Anatomical abbreviations not listed in Fig. 4 captions: cc, circumferential (laminar) canal; ipo, incipient primary osteon. Scale bars: 100 μ m (A, D), 50 μ m (B, C, E, F).

fibrolamellar (Chinsamy and Elzanowski, 2001). Incipient fibrolamellar would be more accurate, were these vascular canals to become infilled. However, due to the lack of lamellae infill and uncertainty that these features would ever become infilled, we refer to these structures simply as large vascular canals and the bone tissue as woven in both IVPP V15686 and *Gobipteryx* ZPAL MgR -/90.

Plump, unorganized osteocyte lacunae (maximum width of 5 μm and maximum length measuring 11 μm) are visible throughout the cross-section. A few smaller longitudinal canals are present in the region of the section with overall lower porosity. Birefringence is nearly absent under polarized light, which may mean that very little collagen is preserved. LAGs, an ICL of endosteal lamellar or parallel fibered bone, and an OCL are all absent.

Based on the presence of woven bone with large vascular canals in some regions that may have been formed *in ovo* based on comparison with *Gobipteryx* ZPAL MgR -/90 and the histology of more mature Jehol enantiornithines, a periosteal surface that is smooth in some regions and weakly scalloped in others, and the overall skeletal immaturity (particularly with regards to the sternum and pygostyle) which classifies this specimen as morphologically early immature, we interpret this specimen as osteohistologically early immature and suggest that IVPP V15686 represents a very young post-hatching individual (Atterholt, 2015; Atterholt and Woodward, 2021).

3.3.3. IVPP V15575B left tibia

The preserved bone is broken into two pieces (Fig. 5(A–C)). As preserved, the bone appears tripartite, formed by two layers of bone with lower vascularity than IVPP V15686 separated by a middle layer consisting of numerous cracks. This middle layer of cracks is interpreted as the approximate position of the endosteal surfaces and the collapsed medullary cavity. The large number of cracks is suggestive of a region with large vascular canals, like those observed in the tibia of IVPP V15686 and *Gobipteryx* ZPAL MgR -/90, in the endosteal-most portion of the cortex that were crushed by post-mortem compaction. If correct, then the measured cortical thickness may represent a slight underestimate in some areas. However, as this is speculative we will focus only on features that can be definitively identified. As in IVPP V15686, the cortex varies (56.9 and 139 μm) so that where it is thickest it measures more than twice the thinnest regions.

The caudal surface faces the matrix but due to missing information regarding the orientation of the section we cannot determine which side represents the medial and lateral directions. The bone contains numerous, large (up to 15.1 μm), irregular osteocyte lacunae together with smaller (minimum 8.6 μm) osteocyte lacunae. Simple longitudinal canals are present throughout, some with a slit-like morphology, which are also observed in IVPP V15686. Several larger longitudinal canals (measuring between 21.6 and 34.55 μm) are present in the thickest region of the cortex, although none are preserved open (fully perforating the section). A few laminar canals may also be present but alternatively may represent cracks. LAGs, an ICL, and an OCL are all absent. The periosteal surface appears weakly scalloped, but the uneven appearance of this surface may be due to poor preservation.

Compared to the tibial section from IVPP V15686, porosity is lower with mostly simple longitudinal canals and very few large vascular canals, which are also in turn smaller on average than those observed in IVPP V15686. Based on the overall lower porosity in both the humeral and tibial sections, we interpret that IVPP V15575 is developmentally more mature than IVPP V15686, although we classify both generally as osteohistologically early immature stage individuals.

3.3.4. IVPP V15575B right humerus

The sample consists of two pieces preserved side by side (Fig. 5(D–F)). Presumably these fragments were originally continuous or nearly so. They are thickest and subequal where they approach each other along the break. An additional small fragment of bone, all that remains of the missing half of the humeral cortex, indicates the endosteal surface of the larger pieces, consistent with the fact the humerus is preserved split between the slab and counter slab (Fig. 5(D)). Since the right humerus is exposed in caudal view in the main slab where sampled, the preserved bone corresponds primarily to the cranial portion of the cortex embedded in the matrix, and the small fragment preserves the endosteal portion of the largely missing caudal half of the humeral cross-section.

In one piece (thickness between 76 and 110 μm) the osteocyte lacunae are plump and irregular (Fig. 5(E)). Both the endosteal and periosteal surfaces are uneven and somewhat scalloped. There are three large, open (fully perforating the section), longitudinal vascular canals (long axis measuring between 20 and 34 μm), three large, slit-like canals, and several smaller canals. The three large canals are dispersed throughout the cortex such that one canal is located very close to the medullary cavity and another approaches the periosteal surface. Lamellae of bone visible around the edges indicate that the inner two canals are incipient primary osteons only partially filled by centripetal bone apposition. It cannot be determined to what degree these incipient primary osteons would later become filled by lamellar bone had bone deposition not been truncated by death (Woodward and Lehman, 2009).

The second piece (thickness 68–109 μm) is nearly avascular and the osteocyte lacunae are much larger (long axis of 20 μm vs. 14 μm in the vascularized fragment and 15 μm in the tibia) and distinctly elongated parallel to the bone surface especially toward the periosteal surface (Fig. 5(F)). One or possibly two laminar (circumferential) canals appear to be present. The periosteal and endosteal surfaces in this piece are both relatively smooth.

In both pieces LAGs, an ICL, and OCL are absent. Differences in porosity and the texture of the endosteal and periosteal surfaces between the two pieces of humeral bone may suggest cortical drift, which is observed in relatively more mature enantiornithines (Atterholt et al., 2021; Cambra-Moo et al., 2006). The flattened osteocyte lacunae in some regions, together with the moderately thinner cortical wall and lower vascular porosity, suggest the bone tissue of the humerus is more mature than that of the tibia. However, this is equivocal without a complete humeral cortex and uncrushed preservation of both elements.

3.4. Ontogenetic changes to skeletal anatomy

The cervical vertebrae are very short (wider than long) in early immature enantiornithines, as noted by Chiappe et al. (2007). When these first early immature specimens were originally described, it was unclear to what degree this was exaggerated by compression and how much these proportions differed from adults (Chiappe et al., 2007). Considering currently available data, these proportions observed in early immature individuals cannot be attributed to compression, since more mature Jehol enantiornithines are similarly compressed, yet show vertebrae that are typically equal in length and width (e.g., *Parapengornis*, *Parabohaiornis*), or longer than wide (e.g. *Pengornis*, *Rapaxavis*), and the vertebral arch does not become noticeably pinched along the midline.

The range of observed interclavicular angles observed in early immature enantiornithines and the presence of a well-developed hypocleidium suggests the morphology of the furcula may be one of the elements that can be relied on to not strongly vary with ontogeny, although this interpretation is equivocal pending an available ontogenetic series. The deltopectoral crest is weakly developed in IVPP V15575, V15686, and most previously described

Table 2
Developmental stages in enantiornithine ontogeny with regards to compound bone formation and osteohistological traits. Abbreviations: 0, unfused; 1, partially fused; 2, nearly fused but suture visible; 3, completely fused; -, not or badly preserved, or not sampled; Y, developed; N, not developed; f, femur; h, humerus; t, tibia; u, ulna.

Stage	Taxon	Collection	Publication	Synsacrum	Pygostyle	Carpometacarpus (proximally)	Tibiotarsus	Tarsometatarsus (proximally)	Histology		
									ICL	OCL	LAG
0a	Enantiornithes sp.	IVPP V15575	This work	0	0	0	0	0	N(t)	N(t)	N(t)
0b	Enantiornithes sp.	IVPP V15686	This work	0	1	0	?	?	N(t)	N(t)	N(t)
0c	Enantiornithes sp.	STM 34-1	Zheng et al. (2012)	0	1	?	0	0	-	-	-
1	<i>Parapengornis eurycaudatus</i>	IVPP V18687	Hu et al. (2015)	-	3	0	0	0	N(f)	N(f)	N(f)
1	<i>Parapengornis eurycaudatus</i>	IVPP V18632	Hu et al. (2014)	3	3	0	0	0	-	-	-
1	<i>Protapteryx jengmingensis</i>	IVPP V11665	Zhang and Zhou (2000)	3	3	0	0/1	0	-	-	-
1	<i>Eopengornis martini</i>	STM 24-1	Wang et al. (2014)	3	3	0	0/1	0	Y(u)	N(u)	N(u)
2a	<i>Monoenantiornis silhedangia</i>	IVPP V20289	Hu and O'Connor (2017)	3	3	0	1	1	Y(h)	Y(h)	Y(h)
2b	<i>Bohaiornis guoi</i>	LPM B00167	Hu et al. (2011)	3	3	0	2	2	Y(f)	Y(f)	Y(f)
2b	<i>Succavis georum</i>	BMNH pH 000,805	O'Connor et al. (2013)	3	3	0/1	2	2	Y(u)	N(u)	N(u)
2b	<i>Parabohaiornis martini</i>	IVPP V18691	Wang et al. (2014)	3	3	0	2	0/1	-	-	-
2b	<i>Parabohaiornis martini</i>	IVPP V18690	Wang et al. (2014)	3	3	-	2	0/1	-	-	-
2b	<i>Longsunguis kurochikini</i>	IVPP V17964	Wang et al. (2014)	3	3	0	2	0/1	-	-	-
3	<i>Zhouornis hani</i>	CNUVB 0903	Zhang et al. (2013)	-	3	3	3	3	Y(f)	N(f)	Y(f)
3	<i>Pengornis houli</i>	IVPP V15336	Zhou et al. (2008)	3	3	3	3	3	-	-	-
3	<i>Pterygornis dapingfangensis</i>	IVPP V20729	Wang et al. (2016)	3	3	3	3	3	-	-	-
3	<i>Fortunguavis xitotaiensis</i>	IVPP V18631	Wang et al. (2014)	3	3	3	3	3	-	-	-

early immature enantiornithines but relatively more developed in the larger in GMV-2159. This suggests that this crest becomes more distinct with advancing ontogenetic maturity, a pattern also observed in the basal ornithuromorph *Archaeorhynchus* (Foth et al., 2021) and extant birds (Watanabe, 2017). The capital groove on the caudal surface of the proximal humerus is weakly developed or absent in early immature enantiornithines and becomes deeper and more prominent in late immature and mature individuals.

The posterior trochanter of the femur does not appear to be developed in IVPP V15686 and this may be a feature that becomes more distinct with advancing maturity. It also appears absent in the only individual in LH 11386 (a pellet consisting of four immature birds; Sanz et al., 2001) in which the proximolateral femur can be observed. In IVPP V12707 there is a longitudinally oriented ridge on the lateral surface that extends the proximal 1/6 of the femur which may represent an early stage in the development of the posterior trochanter. Although it is reported present in GMV-2158 (Chiappe et al., 2007), the femur is broken in the area of this trochanter and its presence cannot be unequivocally confirmed.

A metatarsal IV that is relatively thinner in dorsal view relative to the metatarsals II and III is a synapomorphy of Enantiornithes or a large subset of enantiornithines (Chiappe and Walker, 2002; O'Connor et al., 2011). However, this is absent in IVPP V15575, IVPP V12707, STM34-2 and GMV-2158. This suggests that at least some enantiornithines hatch with plesiomorphic proportions between metatarsals II-IV and the enantiornithine condition only appears with greater ontogenetic maturity. In LH 11386, one individual appears to already have a reduced metatarsal IV but not another. A reduced metatarsal IV is weakly expressed in STM34-1, which has a sternal morphology (cranial midline ossification is well ossified and nearly contacting the caudal midline ossification) that is more mature than most other early immature enantiornithines (Zheng et al., 2012). However, it is worth noting that many mature enantiornithines have metatarsals II and IV that are subequal such that with the currently available data, potential ontogenetic changes in metatarsal proportions are equivocal.

These new specimens additionally allow the sequence in which compound bones form to be refined (Table 2). Differences between IVPP V15575 and V15686 suggest that the pygostyle co-ossifies shortly after hatching, even before the sternum becomes more ossified (Figs. 3, 6). In IVPP V15575, the most morphologically immature documented post-hatching individual to date, none of the compound bones are formed and the sternum consists of four small and widely separated anlagen. However, the pygostyle must begin to coalesce very early in post-hatching ontogeny, as IVPP V15686 has a partially fused pygostyle but a sternum similar to that in IVPP V15575 (Figs. 3, 6). By the time the sternal anlagen begin to approach each other, the vertebrae forming the pygostyle appear to be fully co-ossified although the structure itself is proportionately longer than in mature individuals (e.g., STM34-1). This indicates negative allometric growth of the pygostyle during early ontogeny. The synsacrum is the next compound bone to form, followed by the carpometacarpus, tibiotarsus and tarsometatarsus, which only become fused in mature individuals (Hu and O'Connor, 2017).

4. Discussion

The osteohistological sections from the two early immature enantiornithines described here provide new data that begins to fill a critical gap in our understanding of the early ontogenetic changes in bone tissue formation experienced by this clade. For the first time we provide traditional ground section data on the bone tissue in early immature enantiornithines (Fig. 6). Despite new data, outstanding questions remain and to fully understand

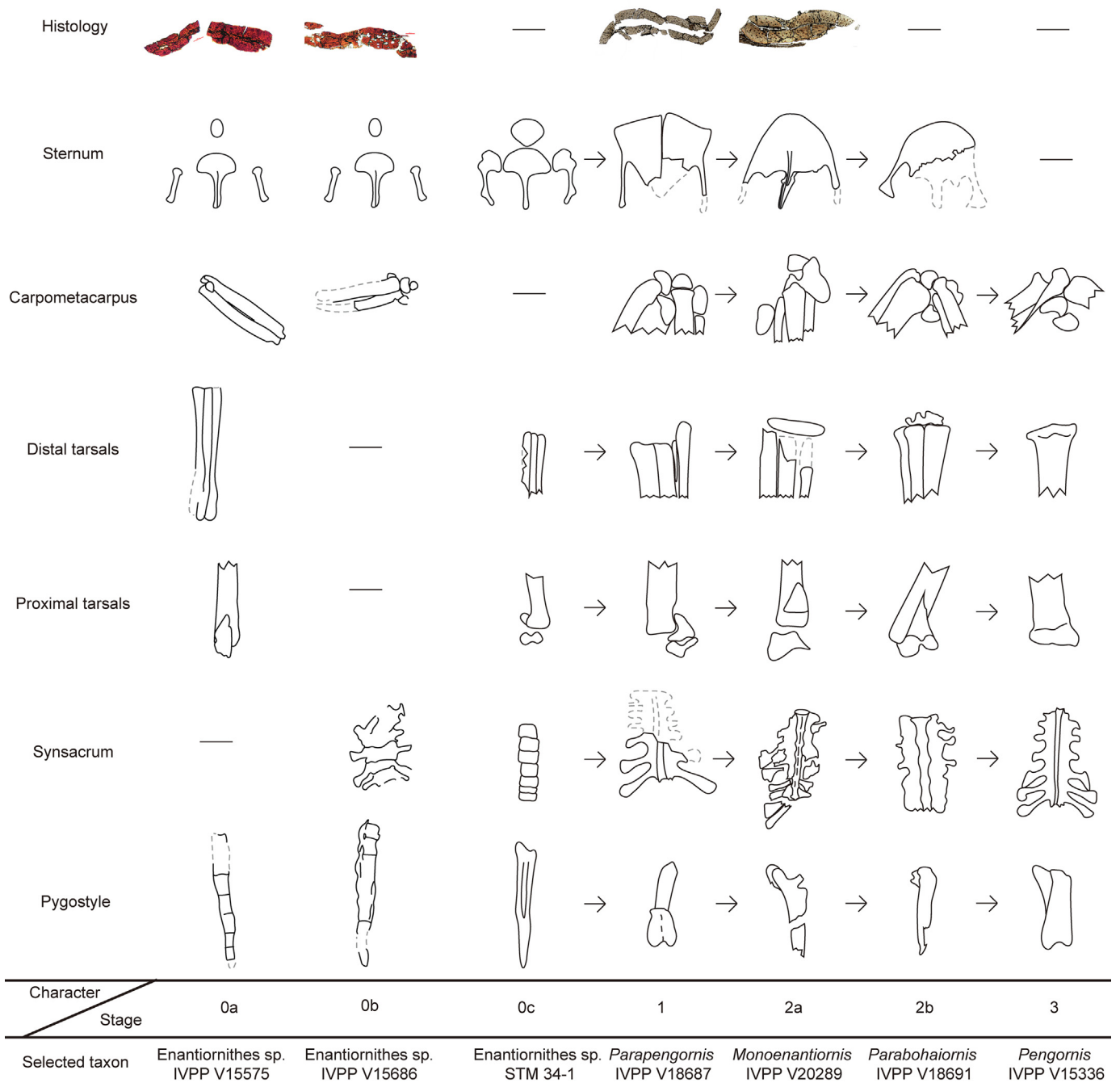


Fig. 6. Illustrations of preserved compound bones of Early Cretaceous enantiornithines across multiple ontogenetic stages revealing the sequence in which fusion events occur in this clade (modified from Hu and O'Connor, 2017).

growth trajectories in this diverse clade far more histological analyses are required across all developmental stages, especially considering the subtle differences in growth strategies inferred from currently available data.

Two osteohistologically and morphologically early immature specimens from the Jehol Group in northeastern China were sampled: IVPP V15575 and V15686. In both specimens the tibia was sampled in order to have homologous sections for comparison with the tibia of ZPAL MGr -/90, a late-stage embryo referable to *Gobipteryx* from the Late Cretaceous of Mongolia (Chinsamy and Elzanowski, 2001). Unfortunately, only a small section of the cortex was published for *Gobipteryx* ZPAL MGr -/90 limiting comparisons.

4.1. Note on *Gobipteryx* ZPAL MGr -/90

According to the published photograph and scale, the tibial cortex in ZPAL MGr -/90 measures between 282–382 μm (Chinsamy and Elzanowski, 2001). Although ZPAL MGr -/90 is very fragmentary such that no long bone elements can be measured, ZPAL MGr -/34, another *Gobipteryx* embryo from the same nesting ground, has an estimated humeral length of 18.7 mm (Elzanowski, 1981). This would suggest a cortical thickness that is approximately 3× greater than that in the similarly sized IVPP V15686 (humeral length 17 mm), a notable and unusual difference. We suggest that the published scale bar in Chinsamy and

Elzanowski (2001) is incorrect. Alternatively, *Gobipteryx* had very thick cortical bone, at least in the tibia, possibly indicating that it did not share the arboreal ecology interpreted for almost all Early Cretaceous enantiornithines. PIN 4492-1 was originally described as the holotype of *Nanantius valifanovi* (Kurochkin, 1996), but is alternatively interpreted by some researchers to represent a mature specimen of *Gobipteryx minuta*; if correct, it is the only mature specimen of *Gobipteryx* preserving postcranial material (Chiappe et al., 2001). The elongate proportions of the tibiotarsus in PIN 4492-1 may suggest *Gobipteryx* was more terrestrial than Early Cretaceous enantiornithines from the Jehol Biota with much thinner tibial cortices. However, size and terrestrial habits of *Gobipteryx* support the interpretation that the scale bar is incorrect because increases in bone density are associated with graviportality and aquatic behaviors (Fabbri et al., 2022), neither which is inferred for *Gobipteryx*.

4.2. Comparison of early immature enantiornithine osteohistology

Woven bone with large vascular canals forms during the late stages of embryonic development in a wide range of vertebrates and is observed in *Gobipteryx* ZPAL MgR -/90 (Chinsamy and Elzanowski, 2001; Horner et al., 2001). In some birds this bone tissue can continue to form after hatching, reflecting continued high growth rates (Atterholt and Woodward, 2021). In late immature and mature enantiornithines, woven bone with substantial amounts of large canals (>3) or primary osteons are not observed indicating that this *in ovo*-formed bone is entirely absorbed by medullary expansion as in modern birds (Atterholt et al., 2021; O'Connor et al., 2014). The data gleaned from IVPP V15575 suggests that growth slowed shortly after hatching in this individual, but was still elevated relative to that observed in enantiornithines that are more than one year old; large vascular canals are still present in the humerus of IVPP V15575, although fewer than observed in embryonic bone (*Gobipteryx* ZPAL MgR -/90) but greater than observed in specimens with LAGs (e.g., STM28-9), which preserve no large canals. The bone tissue in the tibia of IVPP V15686 is more difficult to interpret. There are numerous large canals present but whether this represents embryonic bone or rapidly formed bone deposited after hatching cannot be determined unequivocally.

The histology and patterns of skeletal fusion observed in IVPP V15575 and V15686 suggest these two specimens represent slightly different ontogenetic stages. However, because they likely represent different taxa and interspecific variability in growth patterns is observed in enantiornithines (Atterholt et al., 2021; Chinsamy et al., 1994; O'Connor et al., 2014), and intraspecific variability is inferred, it is impossible to conclusively determine if one specimen is 'older' (in number of days post-hatching) than the other. IVPP V15575, although slightly smaller in size than IVPP V15686, is osteohistologically more mature but morphologically less mature. Relative osteohistological maturity is inferred based on the proportionately lower overall porosity in the tibia of IVPP V15575, as well as the more uniform cortical width of this element. However, the relatively greater degree of fusion between the caudal vertebrae forming the pygostyle in IVPP V15686 indicates that it is morphologically more mature than IVPP V15575.

With its higher porosity and scalloped surfaces, the histology in IVPP V15686 resembles that of the *Gobipteryx* embryo ZPAL MgR -/90 (Chinsamy and Elzanowski, 2001). However, in IVPP V15686 the skeleton is not preserved in a tucked position and there is no evidence of eggshell. Thus, we interpret IVPP V15686 as having perished shortly after hatching. In ZPAL MgR -/90 the periosteal surface is heavily scalloped indicating active growth as in extant hatchling birds (Atterholt, 2015; Atterholt and Woodward, 2021). Unfortunately, because the whole cross section of *Gobipteryx* ZPAL MgR -/90 was not published, it cannot be determined if variation in

vascularity, thickness, and shape of the periosteum like in IVPP V15686 would also be present throughout the cortex.

Compared to ZPAL MgR -/90 and IVPP V15686, the tibia of IVPP V15575 is more similar to the virtual histology published for MPCM-LH-26189 with respect to the degree of porosity (Knoll et al., 2018). However, comparisons with MPCM-LH-26189 are tentative because microanatomical features are not clearly observable from the scan data (virtual cross-sections; Knoll et al., 2018). In IVPP V15575 and MPCM-LH-26189, large vascular canals appear fewer and proportionately smaller compared to ZPAL MgR -/90 and IVPP V15686. In the tibia of MPCM-LH-26189 eight to ten large canals are present, mostly in the inner half of the cortex. No large canals (perforating the section, forming open spaces) are clearly visible in the tibia of IVPP V15575 but a few are present in the humerus. Although the canals in the tibia in IVPP V15575 appear to be close in size to those observed in MPCM-LH-26189, when measured, the average vascular canal area the tibial section of IVPP V15575 is nearly double that of MPCM-LH-26189 on an absolute scale (Table 1). However, the proportionately smaller size of the vascular spaces in these two specimens relative to IVPP V15686 also is reflected in the relatively more even thickness of the cortex in MPCM-LH-26189 and IVPP V15575. Greater vascularization is concentrated in the thicker portions of the cortex in IVPP V15686. Virtual histology prevents identifications of features like lamellae infill so it is impossible to determine if these vascular canals are incipient primary osteons.

4.3. Developmental plasticity in enantiornithines

Growth plasticity has been documented in several non-avian dinosaurs (Chapelle et al., 2021; Sander and Klein, 2005; Woodward et al., 2015). Although not explicitly stated, it is also clearly present in the paravian *Anchiornis*, as evident from the decoupling of size and the number of preserved growth marks observed in osteohistological thin sections (Zheng et al., 2014). It is also documented in the early pygostylian birds *Sapeornis* (Zheng et al., 2014) and *Confuciusornis* (Chinsamy et al., 2020).

Protracted growth is present in the basal ornithuromorph *Archaeorhynchus* (Wang and Zhou, 2016). Although only a single adult specimen of *Archaeorhynchus* (IVPP V20312) has been sampled osteohistologically, size and relative fusion of compound bones are decoupled in immature specimens. *Archaeorhynchus* IVPP V17075 is larger than *Archaeorhynchus* IVPP V17091 but the caudal vertebrae are completely unfused whereas an incipient pygostyle is present in V17091. These data suggest that in early birds, which retain the developmental plasticity characteristic of non-avian dinosaurs, that slight variations in ossification patterns cannot be relied upon to reflect interspecific patterns in indeterminate juvenile enantiornithines. Although no growth series is available for any enantiornithine taxon, nor has more than one specimen referable to the same taxon been osteohistologically sampled, ontogenetic plasticity was likely at least plesiomorphic to this clade. This would suggest that morphological and osteohistological maturity are decoupled in Enantiornithines, which is precisely what is observed in the two sampled early immature enantiornithines described here (IVPP V15575 is morphologically less mature than IVPP V15686 but osteohistologically more mature).

4.4. Comparison with extant birds and support for precocial flight in enantiornithines

Compared to chicks of extant birds, there are several similarities with the osteological details observed in immature enantiornithines. For example, as observed in IVPP V15686, the areas of the cortex that are thinnest also show the lowest porosity, and cor-

tical thickness varies considerably (Atterholt and Woodward, 2021). While the primary orientation of vascularization is difficult to determine in many hatchling neornithines because of the very rapid deposition of bone, precocial hatchlings clearly have predominantly longitudinal vascularization (Atterholt and Woodward, 2021). This predominance of longitudinally-oriented canals is very similar to observations in the early immature enantiornithines studied here (Fig. 7), as well as the previously described embryo ZPAL MgR -/90 (Chinsamy and Elzanowski, 2001). These similarities with regards to vascular orientation in ontogenetically early immature individuals supports the interpretation that these enantiornithine chicks were precocial.

Osteohistological traits in IVPP V15686 and V15575 also resemble those of extant chicks on the more altricial end of the developmental spectrum, but in individuals from later growth stages. The tibia of IVPP V15575 resembles bone of the femur in a Mourning dove (MVZ190779) classified as a “fledgling” based on the state of plumage development. The tibia of IVPP V15686 is similar to the femur of a three-week-old Green-cheeked conure chick (MVA109898) (Fig. 7). This is further evidence of the relative maturity of the bone tissue in the enantiornithine specimens described here-in, and therefore suggestive that this bone is functionally mature enough to withstand the biomechanical demands of active locomotion. However, the minute size of the individuals and degree of skeletal development of the specimens indicates that they died relatively soon after hatching, further supporting an interpretation of these taxa as precocial, and possibly providing some support in favor of precocial flight abilities in these species.

Even from the limited data available on enantiornithines, important differences relative to neornithine chicks also are apparent. However, bone histology is presently unknown in extant megapodes, the only extant avian clade with precocial flight (and the only extant chicks classified as “super-precocial”), thus we are currently restricted to comparisons with extant chicks without precocial flight. It is possible that comparison with megapodes may give way to greater similarities with extant taxa, in light of existing hypotheses that enantiornithines had precocial flight (Xing et al., 2017; Zhou and Zhang, 2004). In extant birds without precocial flight, ranging from precocial to altricial, the bone tissue of the femur is typically more mature than the humerus at hatching (Atterholt and Woodward, 2021). However, in IVPP V15575 the humerus is more mature than the tibia. While the tibia and femur are different elements, this difference does appear to indicate the opposite pattern, of greater maturity in pectoral limb elements compared to pelvic limb elements in at least some enantiornithines. Use of the tibia as a proxy for the femur in this comparison is supported by the fact that the femoral and tibial histology in mature enantiornithines for which both elements have been sectioned show similar tissue structure and cortical thicknesses (O'Connor et al., 2018; Wang et al., 2020). The relative greater maturity of the pectoral limb elements in enantiornithines supports the interpretation that they are precocial flyers, whereas in non-precocial flyers (including both altricial and precocial chicks broadly) the hindlimb becomes histologically mature before the forelimb.

The humeral and tibial cortical thicknesses are similar in both the immature IVPP V15575 and the mature *Mirusavis* IVPP V16892 (Wang et al., 2020). The cortical thickness of the humerus and tibia in IVPP V15575 are relatively similar with the range of values for these two elements overlapping each other considerably (Table 1). The average thickness (calculated by averaging the lower and upper limits of the cortical thickness) of the tibia is 98 μm , which is only slightly greater than that the average thickness of the humerus calculated as 93 μm (humerus is 92% the thickness of the tibia). The same pattern is observed in the adult enantiornithine *Mirusavis* IVPP V18692, in which the average cortical thick-

ness of the humerus (206.5 μm) is 95% that of the tibiotarsus (224.5 μm). The difference is even less when comparing the femur, which has a lower average cortical thickness in IVPP V18692 (222.5 μm ; humerus is 93% the average cortical thickness of the femur). This is consistent with available evidence for precocial birds, in which the forelimb and hindlimb have similar cortical thicknesses (Atterholt and Woodward, 2021). However, extant precocial birds tend to have larger body sizes and utilize predominantly hindlimb locomotion. In contrast, extant arboreal birds typically have more altricial developmental strategies and humeri that tend to be proportionately thicker than the femur in adults (Atterholt and Woodward, 2021). Therefore, when compared to neornithines, enantiornithines exhibit relative proportions of long bone cortical thicknesses that are consistent with their precocial development but contrast with their ecology.

The proportionately similar cortical thicknesses of the forelimb and hindlimb long bones observed in early immature and mature individuals, which contrasts to the proportions observed in extant birds without precocial flight, suggests precocial development of the humerus and tentatively supports the widespread hypothesis that enantiornithines were capable of precocial flight shortly after emerging from the egg. However, preliminary data from a CT scan of an embryo of *Megapodius pritchardi* only somewhat supports this interpretation, revealing a humeral cortex that is in some regions thicker than the femur and tibia. Unfortunately, the scan data does not permit observation of vascularity and no data is available for early immature or mature individuals of this taxon to determine how bone tissue and cortical proportions may change with hatching and ontogenetic maturity. These differences may also reflect phylogeny and or ecology and further data are required.

This further highlights the unique development and ecology of these Cretaceous birds. The more mature bone tissue of the humerus in IVPP V15575 as compared to the tibia, the opposite pattern observed in extant birds is most likely indicative of the functional demand placed on the humerus by precocial flight in enantiornithines. Evidence suggests that hatching with a femur that is histologically more mature than the humerus is plesiomorphic to Neornithes, and possibly even to *Aves sensu Sereno* (2005) (Atterholt and Woodward, 2021); the shift towards greater maturity in the forelimb relative to the hindlimb observed in IVPP V15575 probably reflects the apomorphic evolution of locomotor super-precociality observed in enantiornithines.

4.5. Reassessment of previously described individuals

New information regarding osteohistology in post-hatching enantiornithine individuals suggests that the ontogenetic status and growth strategy of some previously described specimens can now be assessed with greater accuracy. Two previously described enantiornithines were described as having humeri with avascular bone and an absence of LAGs: the holotype specimens of *Cruralispennia multidonta* (Wang et al., 2017b) and *Parvavis chuxiongensis* (Wang et al., 2014). Both these specimens are only slightly larger than the juveniles described here (Table 1). The larger of the two (based on humeral length), *Cruralispennia* IVPP V21711 is 114% the size of IVPP V15575 and 123% the size of IVPP V15686. Reevaluation of the published histological images reveals that the humeral cross-sections of both *Cruralispennia* IVPP V21711 (Wang et al., 2017a, 2017b: suppl. fig. 4) and *Parvavis* V18586 (Wang et al., 2014: fig. 6A) possess at least one large vascular canal. Four to eight smaller canals are additionally present in *Parvavis* IVPP V18586. The presence of large vascular canals in these early immature specimens described here, as well as the late-stage *Gobipteryx* embryo, and their absence in larger enantiornithines that preserve LAGs favors the interpretation of the osteohistology that both these specimens represent individuals in their first year of growth.

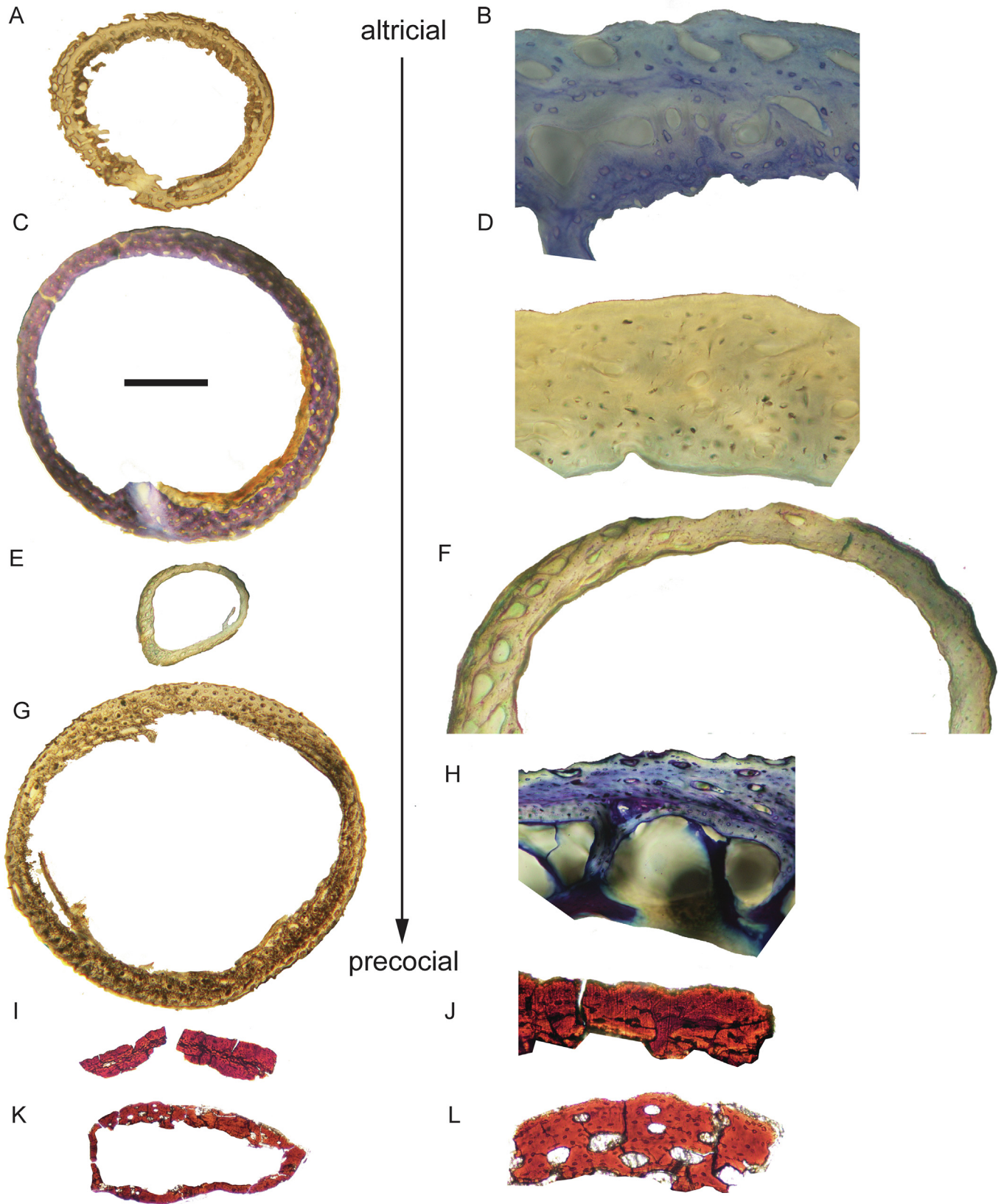


Fig. 7. Comparative perinate osteohistology of neornithines across the developmental spectrum and the two early immature enantiornithines described here. **A, B.** Green-cheeked parakeet/conure (*Pyrrhura molinae*). **C, D.** Mourning dove (*Zenaida macroura*). **E, F.** California quail (*Callipepla californica*). **G, H.** Wild turkey (*Meleagris gallopavo*). **I, J.** enantiornithine indet. IVPP V15575. **K, L.** enantiornithine indet. IVPP V15686 (attempted reconstruction of the tibial cross section; shape not accurate). The complete cross-section and close-up image for each extant taxon do not represent the same section with the exception of *Callipepla*. Scale bar: 500 μ m (A, C, E, G, I, K).

The presence of an ICL and OCL in *Cruralispennia* IVPP V21711 indicates that growth had slowed and that IVPP V21711 is osteohistologically more mature than IVPP V15685 and V15575, consistent with indicators of greater morphological maturity (the morphology of the sternum in this specimen in which the anlagen are fused into a single element; Wang et al., 2017b). However, as noted by other authors, the presence of an OCL does not necessarily indicate morphological or even osteohistological maturity has been achieved (Woodward et al., 2020). Some early immature specimens also preserve immature feathers across the body (O'Connor et al., 2020). These specimens, together with *Cruralispennia* IVPP V21711, hint at unique molt patterns in enantiornithines. Neornithine molt patterns reflect their rapid growth to adult size (Gill, 2007). Given differences in enantiornithine growth it is logical they would have different molt patterns. Super-precocial megapodes have protracted juvenal molts (Wong, 1999) yet available evidence suggests molts in immature enantiornithine were rapid (O'Connor et al., 2023). In contrast to early immature specimens, molting feathers are not present in all regions of the body in *Cruralispennia* IVPP V21711. The evidence from *Cruralispennia* may suggest molts were less rapid approaching morphological maturity. It also may suggest that the OCL and ICL formed in response to the temporary elevation of energetic demands due to molting in IVPP V21711.

5. Conclusions

Interpretations regarding ontogenetic changes in bone deposition in the Enantiornithes are hindered by the very limited available data and differences in the elements sampled between specimens, yet some patterns are beginning to emerge. The overall data suggests that enantiornithines had growth patterns fairly consistent with that of extant birds with differences that likely reflect the unique highly precocial developmental strategy of the Enantiornithes. Osteohistological similarities to extant precocial chicks, the more mature bone tissue observed in the humerus of IVPP V15575, and the similar proportions between the cortical thicknesses of the forelimb and hindlimb long bones observed in both immature and mature specimens all support inferences regarding precocial flight. Greater sampling of enantiornithines at all developmental stages is required to see if these observed patterns are clade wide or lineage specific. Patterns will surely be elucidated through increased sampling not only among the Cretaceous Enantiornithes but also across development of a greater diversity of extant birds. Clearly to understand clades as diverse and with such long evolutionary histories as Enantiornithes and Neornithes, far more data are required.

CRediT authorship contribution statement

Jingmai K. O'Connor: Conceptualization, Formal analysis, Investigation, Resources, Visualization, Writing – original draft, Writing – review & editing. **Jessie Atterholt:** Investigation, Writing – original draft, Writing – review & editing. **Alida M. Bailleul:** Investigation, Writing – review & editing. **Min Wang:** Investigation, Writing – review & editing. **Pei-Chen Kuo:** Investigation, Writing – review & editing. **Zhonghe Zhou:** Funding acquisition, Resources.

Data availability

No data was used for the research described in the article.

Declaration of competing interest

The authors declare that they have no known competing financial interests or personal relationships that could have appeared to influence the work reported in this paper.

Acknowledgements

We thank W. Gao for photographing the specimens and S-K. Zhang for making the ground-sections. We thank D.J. Field for access to the *Megapodius* hatchling. This research was supported by the National Natural Science Foundation of China (41688103, 42288201).

References

- Atterholt, J.A., Hutchison, J.H., O'Connor, J., 2018. The most complete enantiornithine from North America and a phylogenetic analysis of the Avisauridae. *PeerJ* 6, 1–45.
- Atterholt, J.A., Poust, A.W., Erickson, G.M., O'Connor, J.K., 2021. Intraskelletal osteohistovariability reveals complex growth strategies in a Late Cretaceous enantiornithine. *Frontiers in Earth Science* 9, 1–16.
- Atterholt, J.A., Woodward, H.N., 2021. A histological survey of avian post-natal skeletal ontogeny. *PeerJ* 9, 1–47.
- Atterholt, J.A., 2015. A geometric morphometric and histological study of the role of development in avialan evolution, *Integr. Biol.* University of California, Berkeley, 271 p.
- Bailleul, A.M., Ségalen, L., Buscalioni, A.D., Cambra-Moo, O., Cubo, J., 2011. Palaeohistology and preservation of tetrapods from Las Hoyas (Lower Cretaceous, Spain). *Comptes Rendus Palevol* 10, 367–380.
- Bailleul, A.M., Li, Z.-H., O'Connor, J.K., Zhou, Z.-H., 2019a. Origin of the avian predeulatory and evidence of a unique form of cranial kinesis in Cretaceous ornithuromorphs. *Proceedings of the National Academy of Sciences, U.S.A.* 116, 24696–24706.
- Bailleul, A.M., O'Connor, J., Zhang, S.-K., Li, Z.-H., Wang, Q., Lamanna, M., Zhu, X.-F., Zhou, Z.-H., 2019b. An Early Cretaceous enantiornithine (Aves) preserving an unlaid egg and probable medullary bone. *Nature Communications* 10, 1–10.
- Botelho, J.F., Ossa-Fuentes, L., Soto-Acuña, S., Smith-Paredes, D., Nuñez-León, D., Salinas-Saavedra, M., Ruiz-Flores, M., Vargas, A.O., 2014. New developmental evidence clarifies the evolution of wrist bones in the Dinosaur-Bird transition. *PLoS Biology* 12, e1001957.
- Cambra-Moo, O., Buscalioni, A.D., Cubo, J., Castanet, J., Loth, M.-M., de Margerie, E., de Ricqlès, A., 2006. Histological observations of enantiornithine bone (Saurischia, Aves) from the Lower Cretaceous of Las Hoyas (Spain). *Comptes Rendus Palevol* 5, 685–691.
- Chapelle, K.E.J., Botha, J., Choiniere, J.N., 2021. Extreme growth plasticity in the early branching sauripodomorph *Massospondylus carinatus*. *Biology Letters* 17, 1–6.
- Chiappe, L.M., Norell, M., Clark, J., 2001. A new skull of *Gobipteryx minuta* (Aves: Enantiornithes) from the Cretaceous of the Gobi Desert. *American Museum Novitates* 3346, 1–15.
- Chiappe, L.M., Ji, S., Ji, Q., 2007. Juvenile birds from the Early Cretaceous of China: implications for enantiornithine ontogeny. *American Museum Novitates* 3594, 1–46.
- Chiappe, L.M., Walker, C.A., 2002. Skeletal morphology and systematics of the Cretaceous Euenantiornithes (Ornithothoraces: Enantiornithes). In: Chiappe, L.M., Witmer, L.M. (Eds.), *Mesozoic Birds: above the Heads of Dinosaurs*. University of California Press, Berkeley, pp. 240–267.
- Chinsamy, A., Chiappe, L.M., Dodson, P., 1994. Growth rings in Mesozoic birds. *Nature* 368, 196–197.
- Chinsamy, A., Chiappe, L.M., Dodson, P., 1995. Mesozoic avian bone microstructure: physiological implications. *Paleobiology* 21, 561–574.
- Chinsamy, A., Elzanowski, A., 2001. Evolution of growth pattern in birds. *Nature* 412, 402–403.
- Chinsamy, A., Marugán-Lobón, J., Serrano, F.J., Chiappe, L.M., 2020. Osteology and life history of the basal pygostylian *Confuciusornis sanctus*. *The Anatomical Record* 303, 949–962.
- Cubo, J., Buscalioni, A.D., Legendre, L., Bourdon, E., Sanz, J.L., de Ricqlès, A.J., 2022. Palaeohistological inferences of resting metabolic rates in *Concornis* and *Iberomesornis* (Enantiornithes, Ornithothoraces) from the Lower Cretaceous of Las Hoyas (Spain). *Palaeontology* 65, e12583.
- de Ricqlès, A., 1976. Recherches paléohistologiques sur les os longs des tétrapodes VII. - Sur la classification, la signification fonctionnelle et l'histoire des tissus osseux de tétrapodes (deuxième partie). *Annales de Paléontologie (Vertébrés)* 62, 71–126.
- de Ricqlès, A.J., Padian, K., Horner, J.R., Lamm, E.-T., Myhrvold, N., 2003. Osteohistology of *Confuciusornis sanctus* (Theropoda: Aves). *Journal of Vertebrate Paleontology* 23, 373–386.
- Elzanowski, A., 1981. Embryonic bird skeletons from the Late Cretaceous of Mongolia. *Palaeontologica Polonica* 42, 147–179.

- Erickson, G.M., Rauhut, O.W.M., Zhou, Z.-H., Turner, A.H., Inouye, B.D., Hu, D.-Y., Norell, M.A., 2009. Was dinosaurian physiology inherited by birds? Reconciling slow growth in *Archaeopteryx*. *PLoS ONE* 4, e7390.
- Fabbri, M., Navalón, G., Benson, R.B.J., Pol, D., O'Connor, J., Bhullar, B.-A., Erickson, G. M., Norell, M.A., Orkney, A., Lamanna, M.C., Zouhri, S., Becker, J., Emke, A., Dal Sasso, C., Bindellini, G., Maganuco, S., Auditore, M., Ibrahim, N., 2022. Subaqueous foraging among carnivorous dinosaurs. *Nature* 603, 852–857.
- Foth, C., Wang, S.-Y., Spindler, F., Lin, Y., Yang, R., 2021. A juvenile specimen of *Archaeorhynchus* sheds new light on the ontogeny of basal euornithines. *Frontiers in Earth Science* 9, 1–19.
- Francillon-Viellet, H., De Buffrénil, V., Castanet, J., Géraudie, J., Meunier, F.J., Sire, J.Y., Zylberberg, L., De Ricqlès, A.J., 1990. Microstructure and mineralization of vertebrate skeletal tissues. In: Carter, J.G. (Ed.), *Skeletal Biomineralization: Patterns, Processes and Evolutionary Trends*. Van Nostrand Reinhold, New York, pp. 471–530.
- Gao, C.-H., Chiappe, L.M., Zhang, F.-J., Pomeroy, D.L., Shen, C.-Z., Chinsamy, A., Walsh, M.O., 2012. A subadult specimen of the Early Cretaceous bird *Sapeornis chaoyangensis* and a taxonomic reassessment of sapeornithids. *Journal of Vertebrate Paleontology* 32, 1103–1112.
- Gill, F.B., 2007. *Ornithology*. W.H. Freeman and Company, New York.
- Griffith, C.T., Stocker, M.R., Colleary, C., Stefanic, C.M., Lessner, E.J., Riegler, M., Formoso, K., Koeller, K., Nesbitt, S.J., 2021. Assessing ontogenetic maturity in extinct saurian reptiles. *Biological Reviews* 96, 470–525.
- Horner, J.R., Padian, K., De Ricqlès, A.J., 2001. Comparative osteohistology of some embryonic and perinatal archosaurs: developmental and behavioral implications for dinosaurs. *Paleobiology* 27, 39–58.
- Hou, L., Chen, P., 1999. *Liaoxiornis delicatus* gen. et sp. nov., the smallest Mesozoic bird. *Chinese Science Bulletin* 44, 834–838.
- Hu, D.-Y., Li, L., Hou, L.-H., Xu, X., 2011. A new enantiornithine bird from the Lower Cretaceous of western Liaoning, China. *Journal of Vertebrate Paleontology* 31, 154–161.
- Hu, H., O'Connor, J.K., 2017. First species of Enantiornithes from Sihedang elucidates skeletal development in Early Cretaceous enantiornithines. *Journal of Systematic Palaeontology* 15, 909–926.
- Hu, H., O'Connor, J.K., Zhou, Z.-H., 2015. A new species of Pengornithidae (Aves: Enantiornithes) from the Lower Cretaceous of China suggests a specialized scansorial habitat previously unknown in early birds. *PLoS ONE* 10, e0126791.
- Hu, H., Zhou, Z.-H., O'Connor, J.K., 2014. A subadult specimen of Pengornis and character evolution in Enantiornithes. *Vertebrata Palasiatica* 52, 77–97.
- Huttenlocker, A.K., Woodward, H.N., Hall, B.K., 2013. The biology of bone. In: Padian, K., Lamm, E.-T. (Eds.), *Bone Histology of Fossil Tetrapods*. University of California Press, Berkeley, pp. 13–34.
- Ji, Q., Ji, S., 1999. A new genus of the Mesozoic birds from Lingyuan, Liaoning, China. *Chinese Geology* 26, 45–48.
- Knoll, F., Chiappe, L.M., Sanchez, S., Garwood, R.J., Edwards, N.P., Wogelius, R.A., Sellers, W.I., Manning, P.L., Ortega, F., Serrano, F.J., Marugán-Lobón, J., Cuesta, E., Escaso, F., Sanz, J.L., 2018. A diminutive perinate European Enantiornithes reveals an asynchronous ossification pattern in early birds. *Nature Communications* 9, 1–9.
- Kurochkin, E.N., 1996. A new enantiornithid of the Mongolian Late Cretaceous, and a general appraisal of the Infraclass Enantiornithes (Aves). *Russian Academy of Sciences, Palaeontological Institute, Special Issue*, pp. 1–50.
- O'Connor, J.K., Chiappe, L.M., Bell, A., 2011. Pre-modern birds: avian divergences in the Mesozoic. In: Dyke, G.D., Kaiser, G. (Eds.), *Living Dinosaurs: the Evolutionary History of Birds*. J. Wiley & Sons, Hoboken, NJ, pp. 39–114.
- O'Connor, J., Erickson, G.M., Norell, M.A., Bailleul, A.M., Hu, H., Zhou, Z.-H., 2018. Medullary bone in an Early Cretaceous enantiornithine bird and discussion regarding its identification in fossils. *Nature Communications* 9, 5169.
- O'Connor, J., Falk, A.R., Wang, M., Zheng, X.-T., 2020. First report of immature feathers in juvenile enantiornithines from the Early Cretaceous Jehol avifauna. *Vertebrata Palasiatica* 58, 24–44.
- O'Connor, J.K., Wang, M., Zheng, X.-T., Wang, X.-L., Zhou, Z.-H., 2014. The histology of two female Early Cretaceous birds. *Vertebrata Palasiatica* 52, 112–128.
- O'Connor, J.K., Wang, M., Zhou, S., Zhou, Z.-H., 2015a. Osteohistology of the Lower Cretaceous Yixian Formation ornithomorph (Aves) *Iteravis huchzermeyeri*. *Palaeontologica Electronica* 18 (2), 11 p.
- O'Connor, J.K., Zhang, Y.-G., Chiappe, L.M., Meng, Q.-J., Li, Q.-G., Liu, D., 2013. A new enantiornithine from the Yixian Formation with the first recognized avian enamel specialization. *Journal of Vertebrate Paleontology* 33, 1–12.
- O'Connor, J.K., Zheng, X.-T., Wang, X.-L., Zhang, X.-M., Zhou, Z.-H., 2015b. The gastral basket in basal birds and their close relatives: size and possible function. *Vertebrata Palasiatica* 53, 133–152.
- O'Connor, J.K., Kiat, Y., Ma, H.-D., Ai, T.-Y., Wang, L.-H., Bi, S.-D., 2023. Immature feathers preserved in Burmite provide evidence of rapid molting in enantiornithines. *Cretaceous Research* 149, 105572.
- Pan, Y.-H., Sha, J.-G., Zhou, Z.-H., Fürsich, F.T., 2013. The Jehol Biota: Definition and distribution of exceptionally preserved relicts of a continental Early Cretaceous ecosystem. *Cretaceous Research* 44, 30–38.
- Prondvai, E., Godefroit, P., Adriaens, D., Hu, D.-Y., 2018. Intraskelatal histovariability, allometric growth patterns, and their functional implications in bird-like dinosaurs. *Scientific Reports* 8, 258.
- Sander, P.M., Klein, N., 2005. Developmental plasticity in the life history of a prosauropod dinosaur. *Science* 310, 1800–1802.
- Sanz, J.L., Chiappe, L.M., Pérez-Moreno, B., Moratalla, J.J., Hernández-Carrasquilla, F., Buscalioni, A.D., Ortega, F., Poyato-Ariza, F.J., Rasskin-Gutman, D., Martínez-Delclòs, X., 1997. A nestling bird from the Lower Cretaceous of Spain: implications for avian skull and neck evolution. *Science* 276, 1543–1546.
- Sanz, J.L., Chiappe, L.M., Fernández-Jalvo, Y., Ortega, F., Sánchez-Chillon, B., Poyato-Ariza, F.J., Pérez-Moreno, B.P., 2001. An Early Cretaceous pellet. *Nature* 409, 998–999.
- Sereno, P.C., 2005. The logical basis of phylogenetic taxonomy. *Systematic Biology* 54, 595–619.
- Starck, J.M., Ricklefs, R.E., 1998. Patterns of development: the altricial-precocial spectrum. In: Starck, J.M., Ricklefs, R.E. (Eds.), *Avian Growth and Development*. Oxford University Press, New York City, pp. 3–30.
- Tumarkin-Deratzian, A.R., Vann, D.R., Dodson, P., 2006. Bone surface texture as an ontogenetic indicator in long bones of the Canada goose *Branta canadensis* (Anseriformes: Anatidae). *Zoological Journal of the Linnean Society* 148, 133–168.
- Wang, M., Stidham, T.A., Li, Z.-H., Xu, X., Zhou, Z.-H., 2021. Cretaceous bird with dinosaur skull sheds light on avian cranial evolution. *Nature Communications* 12, 3890.
- Wang, M., Zhou, Z.-H., 2016. A new adult specimen of the basalmost ornithomorph bird *Archaeorhynchus spathula* (Aves: Ornithomorphia) and its implications for early avian ontogeny. *Journal of Systematic Palaeontology* 15, 1–18.
- Wang, M., Stidham, T.A., Zhou, Z.-H., 2018. A new clade of basal Early Cretaceous pygostylian birds and developmental plasticity of the avian shoulder girdle. *Proceedings of the National Academy of Sciences, U.S.A.* 115, 10708–10713.
- Wang, M., O'Connor, J.K., Bailleul, A.M., Li, Z.-H., 2020. Evolution and distribution of medullary bone: evidence from a new Early Cretaceous enantiornithine bird. *National Science Review* 7, 1068–1078.
- Wang, M., Zhou, Z.-H., 2017. The evolution of birds with implications from new fossil evidences. In: Maina, J.N. (Ed.), *The Biology of the Avian Respiratory System: Evolution, Development, Structure and Function*. Springer, Switzerland, pp. 1–26.
- Wang, M., Zhou, Z.-H., Xu, G.-H., 2014. The first enantiornithine bird from the Upper Cretaceous of China. *Journal of Vertebrate Paleontology* 34, 135–145.
- Wang, M., Wang, X.-L., Wang, Y., Zhou, Z.-H., 2016. A new basal bird from China with implications for morphological diversity in early birds. *Scientific Reports* 6, 19700.
- Wang, M., Hu, H., Li, Z.-H., 2016. A new small enantiornithine bird from the Jehol Biota, with implications for early evolution of avian skull morphology. *J Syst Palaeontol* 14, 481–497.
- Wang, M., Li, Z.-H., Zhou, Z.-H., 2017a. Insight into the growth pattern and bone fusion of basal birds from an Early Cretaceous enantiornithine bird. *Proceedings of the National Academy of Sciences, U.S.A.* 114, 11470–11475.
- Wang, M., O'Connor, J.K., Pan, Y.-H., Zhou, Z.-H., 2017b. A bizarre Early Cretaceous enantiornithine bird with unique crural feathers and an ornithomorph plough-shaped pygostyle. *Nature Communications* 8, 14141.
- Watanabe, J., 2017. Ontogeny of macroscopic morphology of limb bones in modern aquatic birds and their implications for ontogenetic ageing. *Contribuciones Del MACN* 7, 183–220.
- Wong, S., 1999. *Development and Behaviour of Hatchlings of the Australian Brush-turkey *Alectura lathami**. Griffith University, Brisbane.
- Woodward, H.N., Fowler, E.A.F., Farlow, J.O., Horner, J.R., 2015. *Maiaasaura*, a model organism for extinct vertebrate population biology: a large sample statistical assessment of growth dynamics and survivorship. *Paleobiology* 41, 503–527.
- Woodward, H.N., Lehman, T.M., 2009. Bone histology and microanatomy of *Alamosaurus sanjuanensis* (Sauropoda: Titanosauria) from the maastrihtian of Big Bend National Park, Texas. *Journal of Vertebrate Paleontology* 39, 807–821.
- Woodward, H.N., Horner, J.R., Farlow, J.O., 2014. Quantification of intraskelatal histovariability in *Alligator mississippiensis* and implications for vertebrate osteohistology. *PeerJ* 2, e422.
- Woodward, H.N., Tremaine, K., Williams, S.A., Zanno, L.E., Horner, J.R., Myhrvold, N. P., 2020. Growing up *Tyrannosaurus rex*: Osteohistology refutes the pygmy “*Nanotyrannus*” and supports ontogenetic niche partitioning in juvenile *Tyrannosaurus*. *Science Advances* 6, eaax6250.
- Wu, Q., Bailleul, A.M., Li, Z.-H., O'Connor, J.K., Zhou, Z.-H., 2021. Osteohistology of the scapuloacromioid of *Confuciusornis* and preliminary analysis of the shoulder joint in Aves. *Frontiers in Earth Science* 9, 1–16.
- Xing, L.-D., O'Connor, J.K., McKellar, R.C., Chiappe, L.M., Tseng, K.-W., Li, G., Bai, M., 2017. A mid-Cretaceous enantiornithine (Aves) hatchling preserved in Burmese amber with unusual plumage. *Gondwana Research* 49, 264–277.
- Yang, S.-H., He, H.-Y., Jin, F., Zhang, F.-C., Wu, Y.-B., Yu, Z.-Q., Li, Q.-L., Wang, M., O'Connor, J.K., Deng, C.-L., Zhu, R.-X., Zhou, Z.-H., 2020. The appearance and duration of the Jehol Biota: Constraint from SIMS U-Pb zircon dating for the Huajiyi Formation in northern China. *Proceedings of the National Academy of Sciences, U.S.A.* 117, 14299–14305.
- Zhang, Z.-H., Chiappe, L.M., Han, G., Chinsamy, A., 2013. A large bird from the Early Cretaceous of China: new information on the skull of enantiornithines. *Journal of Vertebrate Paleontology* 33, 1176–1189.
- Zhang, F., Hou, L., Ouyang, L., 1998. Osteological microstructure of *Confuciusornis*: preliminary report. *Vertebrata Palasiatica* 36, 126–135.

- Zheng, X.-T., Wang, X.-L., O'Connor, J.K., Zhou, Z.-H., 2012. Insight into the early evolution of the avian sternum from juvenile enantiornithines. *Nature Communications* 3, 1116.
- Zhang, F., Zhou, Z., 2000. A primitive enantiornithine bird and the origin of feathers. *Science* 290, 1955–1960.
- Zheng, X.-T., O'Connor, J.K., Wang, X.-L., Wang, M., Zhang, X.-M., Zhou, Z.-H., 2014. On the absence of sternal elements in Anchiornis (Paraves) and Sapeornis (Aves) and the complex early evolution of the avian sternum. *Proceedings of the National Academy of Sciences, U.S.A.* 111, 13900–13905.
- Zhou, Z., Clarke, J., Zhang, F., 2008. Insight into diversity, body size and morphological evolution from the largest Early Cretaceous enantiornithine bird. *Journal of Anatomy* 212, 565–577.
- Zhou, Z., Zhang, F., 2004. A precocial avian embryo from the Lower Cretaceous of China. *Science* 306, 653.
- Zhou, S., Zhou, Z.-H., O'Connor, J.K., 2013. Anatomy of the Early Cretaceous *Archaeorhynchus spathula*. *Journal of Vertebrate Paleontology* 33, 141–152.